Cell Reports

Article

ACSL4-associated lipid metabolism is a distinct therapeutic vulnerability in *KMT2A*-rearranged acute myeloid leukemia

Graphical abstract

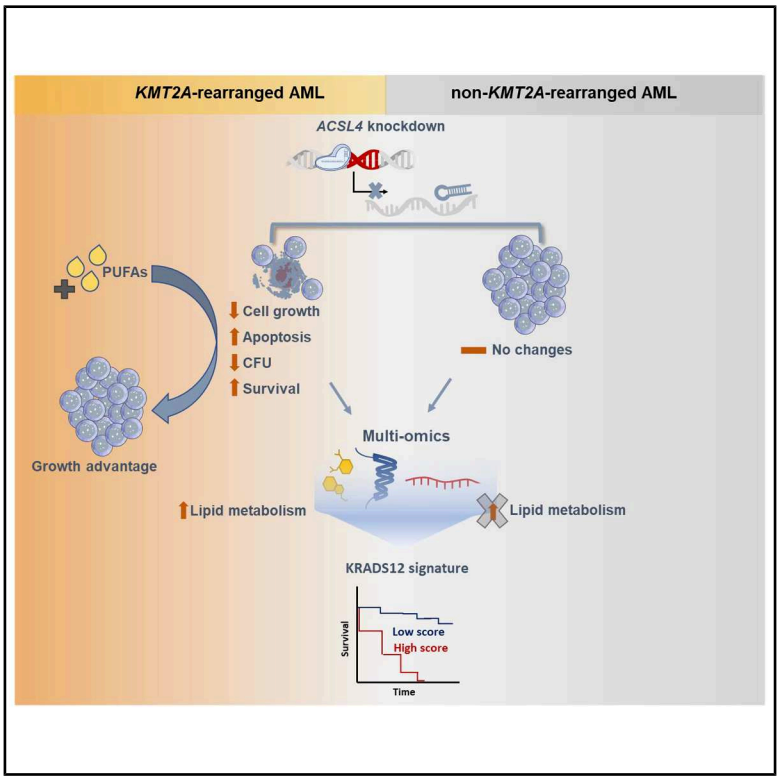

Authors

Silvia Schäfer, Elahe Rahimian, Lola Schmitz-Hübsch, ..., Meritxell Alberich-Jorda, Marius Bill, Alexander A. Wurm

Correspondence

alexander.wurm@nct-dresden.de

In brief

Schäfer et al. identify *ACSL4* as a selective vulnerability in *KMT2A*-rearranged AML. *ACSL4* knockdown impairs leukemic growth *in vitro* and *in vivo* by reprogramming lipid metabolism, which can be rescued by polyunsaturated fatty acids (PUFAs). A KRADS12 signature derived from *ACSL4*-dependent cells is associated with poor patient survival.

Highlights

- *ACSL4* is selectively essential in *KMT2A*r AML cells
- *ACSL4* depletion impairs growth, colony formation, and leukemia expansion *ex vivo* and *in vivo*
- Polyunsaturated fatty acid supplementation rescues growth defects caused by *ACSL4* knockdown
- KRADS12 signature reflects *ACSL4* dependency in *KMT2A*r AML and predicts poor patient survival

Schäfer et al., 2026, Cell Reports *45*, 117010
March 24, 2026
https://doi.org/10.1016/j.celrep.2026.117010

CellPress

Cell Reports

CellPress
OPEN ACCESS

Article

ACSL4-associated lipid metabolism is a distinct therapeutic vulnerability in *KMT2A*-rearranged acute myeloid leukemia

Silvia Schäfer,[1,2,15] Elahe Rahimian,[1,2,3,4,15] Lola Schmitz-Hübsch,[1,2] Mehak Shaikh,[5,6] Silke Brilloff,[1,2,3,4] Vida Kufrin,[1,2,3,4] Sandra Küchler,[1,2,3,4] Maria Fedorova,[7] Natalie Kusebauch,[7] Zhixu Ni,[7] Dominic Helm,[8] Irmela Jeremias,[9] Denis M. Schewe,[3] Claudia R. Ball,[2,10] Martin Bornhäuser,[1,4] Hanno Glimm,[2,11,12,13] Meritxell Alberich-Jorda,[5,14] Marius Bill,[1,2,4,12,16] and Alexander A. Wurm[1,2,3,12,16,17,*]

[1]Mildred Scheel Early Career Center, National Center for Tumor Diseases (NCT/UCC) Dresden, Faculty of Medicine and University Hospital Carl Gustav Carus, TUD Dresden University of Technology, Dresden, Germany
[2]Department for Translational Medical Oncology, National Center for Tumor Diseases Dresden (NCT/UCC), a Partnership between DKFZ, Faculty of Medicine and University Hospital Carl Gustav Carus, TUD Dresden University of Technology, and Helmholtz-Zentrum Dresden - Rossendorf (HZDR), Dresden, Germany
[3]Department of Pediatric Hematology and Oncology, University Hospital Dresden, Dresden, Germany
[4]Department of Internal Medicine I, University Hospital Carl Gustav Carus, TU Dresden University of Technology, Dresden, Germany
[5]Laboratory of Hemato-oncology, Institute of Molecular Genetics of the Czech Academy of Sciences, Prague, Czech Republic
[6]Faculty of Science, Charles University, Prague, Czech Republic
[7]Center of Membrane Biochemistry and Lipid Research, University Hospital and Faculty of Medicine Carl Gustav Carus of TU Dresden, Dresden, Germany
[8]Proteomics Core Facility, German Cancer Research Center (DKFZ), Heidelberg, Germany
[9]Department of Pediatrics, Dr. Von Hauner Children's Hospital, LMU University Hospital, LMU Munich, Munich, Germany
[10]TUD Dresden University of Technology, Faculty of Biology, Dresden, Germany
[11]Translational Medical Oncology, Faculty of Medicine and University Hospital Carl Gustav Carus, TUD Dresden University of Technology, Dresden, Germany
[12]German Cancer Consortium (DKTK), Partner Site Dresden, Dresden, Germany
[13]Translational Functional Cancer Genomics, German Cancer Research Center (DKFZ), Heidelberg, Germany
[14]Childhood Leukaemia Investigation Prague, Department of Pediatric Haematology and Oncology, 2nd Faculty of Medicine, Charles University in Prague, University Hospital Motol, Prague, Czech Republic
[15]These authors contributed equally
[16]Senior author
[17]Lead contact
*Correspondence: alexander.wurm@nct-dresden.de
https://doi.org/10.1016/j.celrep.2026.117010

SUMMARY

Deregulated lipid metabolism contributes to leukemogenesis and the progression of acute myeloid leukemia (AML). By analyzing large-scale CRISPR-Cas9 screening data, we identified acyl-CoA synthetase long-chain family member 4 (*ACSL4*) as a selective vulnerability in lysine methyltransferase 2A-rearranged (*KMT2A*r) AML. Functional validation using CRISPR interference and short hairpin RNA knockdown confirmed that *ACSL4* loss impairs the growth of *KMT2A*r but not non-*KMT2A*r AML cells. *ACSL4* knockdown reduced colony formation in cells derived from patients with *KMT2A*r AML and murine MLL-AF9 cells and delayed leukemia onset *in vivo* in MLL-AF9 mice. A multi-omics approach, including transcriptomics, proteomics, and lipidomics, revealed depletion of polyunsaturated lipid species and compensatory activation of lipid metabolic pathways upon *ACSL4* loss. Supplementation with exogenous polyunsaturated fatty acids (PUFAs) rescued the growth defect, linking *ACSL4* dependency to defective PUFA utilization. Finally, we generated a *KMT2Ar-ACSL4* dependency signature (KRADS12) that correlates with *KMT2A*r status and predicts poor survival in patients with AML.

INTRODUCTION

Acute myeloid leukemia (AML) is a heterogeneous disease of the hematopoietic system characterized by the clonal expansion of undifferentiated myeloid progenitor cells.[1] While standard therapy regimens have remained largely unchanged in recent decades, new, more personalized treatment options have been introduced in the clinic, showing promising results.[2,3] However, the success of these treatment strategies depends on identifying appropriate biomarkers and achieving optimal molecular

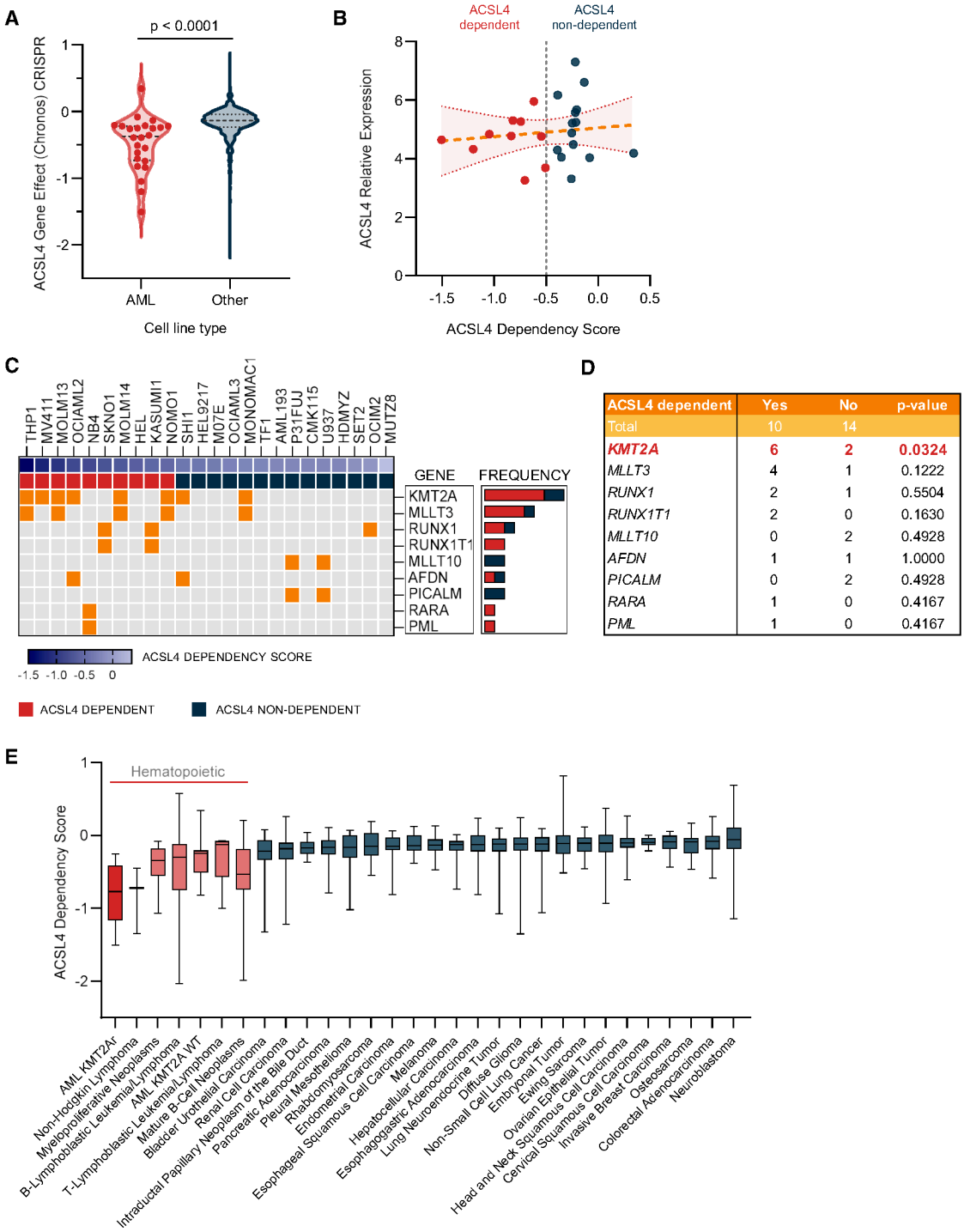

ACSL4 dependent	Yes	No	p-value
Total	10	14	
KMT2A	**6**	**2**	**0.0324**
MLLT3	4	1	0.1222
RUNX1	2	1	0.5504
RUNX1T1	2	0	0.1630
MLLT10	0	2	0.4928
AFDN	1	1	1.0000
PICALM	0	2	0.4928
RARA	1	0	0.4167
PML	1	0	0.4167

Figure 1. Functional genomics identifies *ACSL4* as a potential target in *KMT2A*r AML

(A) Analysis of the DepMap's public genome-scale CRISPR-Cas9 23Q4 (Chronos) essentiality screen dataset comparing the *ACSL4*-dependency of AML cell lines ($n = 24$) to cancer cell lines of other entities ($n = 1076$). Dashed and dotted lines indicate median and quartiles, respectively. p value was calculated based on a two-tailed Mann-Whitney test.

(B) Correlative analysis of *ACSL4* expression and dependency score of the annotated AML cell lines in the DepMap essentiality screen dataset. A threshold of −0.5 was used to divide AML cell lines into *ACSL4*-dependent ($n = 10$) and *ACSL4*-independent ($n = 14$) groups. The calculated Pearson correlation coefficient was r = 0.1214.

(legend continued on next page)

subtype stratification. Approximately 50% of patients with AML carry chromosomal aberrations such as inversions or translocations.[4] One of the most common chromosomal rearrangements in AML involves the lysine methyltransferase 2A (*KMT2A*) gene, formerly known as mixed-lineage leukemia (*MLL*). Depending on the fusion partner, *KMT2A* rearranged (*KMT2A*r) AML is considered an intermediate risk (t(9;11) (p21.3;q23.3)/*MLLT3*::*KMT2A*) or adverse risk (t(v;11q23.3)/*KMT2A* rearranged) according to the European LeukemiaNet (ELN) risk classification.[5] *KMT2A*r is found in 5%–10% of children and adults and 60%–70% of infants with acute leukemia.[6,7] As a histone methyltransferase, *KMT2A* is involved in the epigenetic regulation of various target genes. Rearrangements of *KMT2A* induce aberrant expression of *HOX* genes, resulting in a blockade of hematopoietic differentiation and leukemogenesis.[8] As *KMT2A*r AML is a heterogeneous disease, personalized treatment options as well as novel therapeutic targets are of great need.

Fatty acid (FA) metabolism is a critical process for energy production in dividing AML cells.[9,10] FAs are catabolized by a process called fatty acid oxidation (FAO), which is facilitated by multiple enzymes.[11] Pharmacological inhibition of FAO has previously been shown to induce apoptosis in AML cells.[12] Before FAO takes place, free FAs must enter the mitochondrial matrix, which is enabled by an enzymatic activation. The family of long-chain acyl-CoA synthetases (ACSLs) catalyzes the activation of long-chain FAs by converting free long-chain FAs (chain length of 8–22 carbons) into fatty acyl-CoA esters. Acyl-CoA synthetase long-chain family member 4 (ACSL4) is an isoenzyme of the ACSL family and prefers 20-carbon polyunsaturated fatty acids (PUFAs) as substrates.[13] PUFAs are required for many biological processes, such as energy production, biological membrane structure, and cell signaling pathways.[14–16] However, a dysregulated expression of enzymes involved in PUFA metabolism is a common feature in different cancer entities.[17–19]

ACSL4 has been reported to either promote[20,21] or suppress tumor growth[22,23] in different solid cancers. In healthy hematopoiesis, ACSL4 has been reported to be involved in maintaining hematopoietic stem and multipotent progenitor cells (HSPCs) during iron restriction.[24] Altogether, different publications suggest that *ACSL4* has a tumor-promoting or -suppressing role and a stem cell-maintaining function. However, the role of *ACSL4* in AML warrants further investigation and could represent a promising target for AML treatment.

In this study, we report *ACSL4* as a selective dependency in *KMT2A*r AML. *ACSL4* knockdown impairs colony formation in human patient-derived AML models and primary murine cells and delays leukemia progression in a *KMT2A*r mouse model. In a multi-omics analysis using transcriptomics, proteomics, and lipidomics, we demonstrate an upregulation of lipid metabolism pathways to compensate for *ACSL4* loss exclusively in *KMT2A*r AML. Notably, PUFAs supplementation rescues the growth defect caused by *ACSL4* loss in *KMT2A*r cells, confirming its functional dependency. Lastly, we show that a high score of a 12-gene-containing *KMT2A*r-*ACSL4* dependency signature is a predictor for poor outcome in patients with AML.

RESULTS

Functional genomics identifies *ACSL4* as a potential target in *KMT2A*r AML

To investigate *ACSL4* as a potential target in AML, we performed a comprehensive analysis using the DepMap public genome-scale CRISPR-Cas9 23Q4 (Chronos) essentiality screen dataset. Here, the dependency of a single cell line on the vast majority of known protein-coding genes has been assessed and is reflected by a distinct dependency score for each gene in more than 1,000 cancer cell lines. A score of 0 indicates a non-essential gene, whereas a score of −1 represents the median of all common essential genes.[25] We evaluated this score for *ACSL4* across all included cell lines and observed a significantly stronger effect in AML compared to cell lines from other cancer entities (Figure 1A). A further stratification within the AML subset revealed a distribution of cell lines with lower and higher dependency on *ACSL4*, with dependency score ranging from −1.5 to +0.3. As a first step, we correlated *ACSL4* dependency with *ACSL4* expression and therefore divided the AML cell lines into two groups: *ACSL4*-dependent (dependency score < −0.5) and non-*ACSL4*-dependent (dependency score > −0.5). Interestingly, *ACSL4* expression did not correlate with *ACSL4* dependency and consequently cannot predict *ACSL4* dependency (Figure 1B). To identify molecular differences between *ACSL4*-dependent and non-dependent cell lines, we compared the mutational landscape between these two groups (Figure S1A; Table S1A). Here, we did not find a significant difference in the frequency of single gene mutations. Since single gene alterations are not as frequent in AML as in other cancer entities,[4] we also considered differences in other genomic abnormalities as a possible explanation for the selective *ACSL4* dependency in AML. Therefore, we analyzed DepMap's Fusions Public 23Q4 dataset and performed a statistical analysis of the most common clinically relevant gene fusions in our selected AML cell lines (Figures 1C and 1D; Table S1B). Interestingly, we discovered a significantly higher prevalence of fusions involving the *KMT2A* gene in *ACSL4*-dependent cell lines compared to non-*ACSL4*-dependent cell lines (Figures 1D and S1B). Further, when defining *KMT2A*r AML as a distinct disease group of cell lines, it exhibited the lowest *ACSL4* dependency score compared to all other hematopoietic and non-hematopoietic cancer entities (Figure 1E; Table S1C). In addition to the DepMap dataset, other published CRISPR genome-wide datasets reveal similar results: an increased dependency on *ACSL4* in *KMT2A*r AML cell lines or mouse models compared to *KMT2A* wild-type (WT) samples (Figure S1C).[26,27] Gene set enrichment analysis (GSEA) of cell lines with high vs. low *ACSL4* dependency further supported our findings, indicating upregulated *MLL* (*KMT2A*) gene signatures in

(C) Oncoplot illustrating the most frequent AML-associated fusion genes in different AML cell lines. The cell lines are sorted by their *ACSL4* dependency score. Orange-filled squares indicate a fusion of the indicated gene in the respective cell line.
(D) Statistical analysis of gene fusions depicted in (C), comparing the frequency of fusions in *ACSL4*-dependent or independent AML cell lines. *p* value was calculated based on a Fisher's exact test.
(E) *ACSL4* dependency of cell lines of different cancer entities analyzed using the DepMap's essentiality screen dataset.

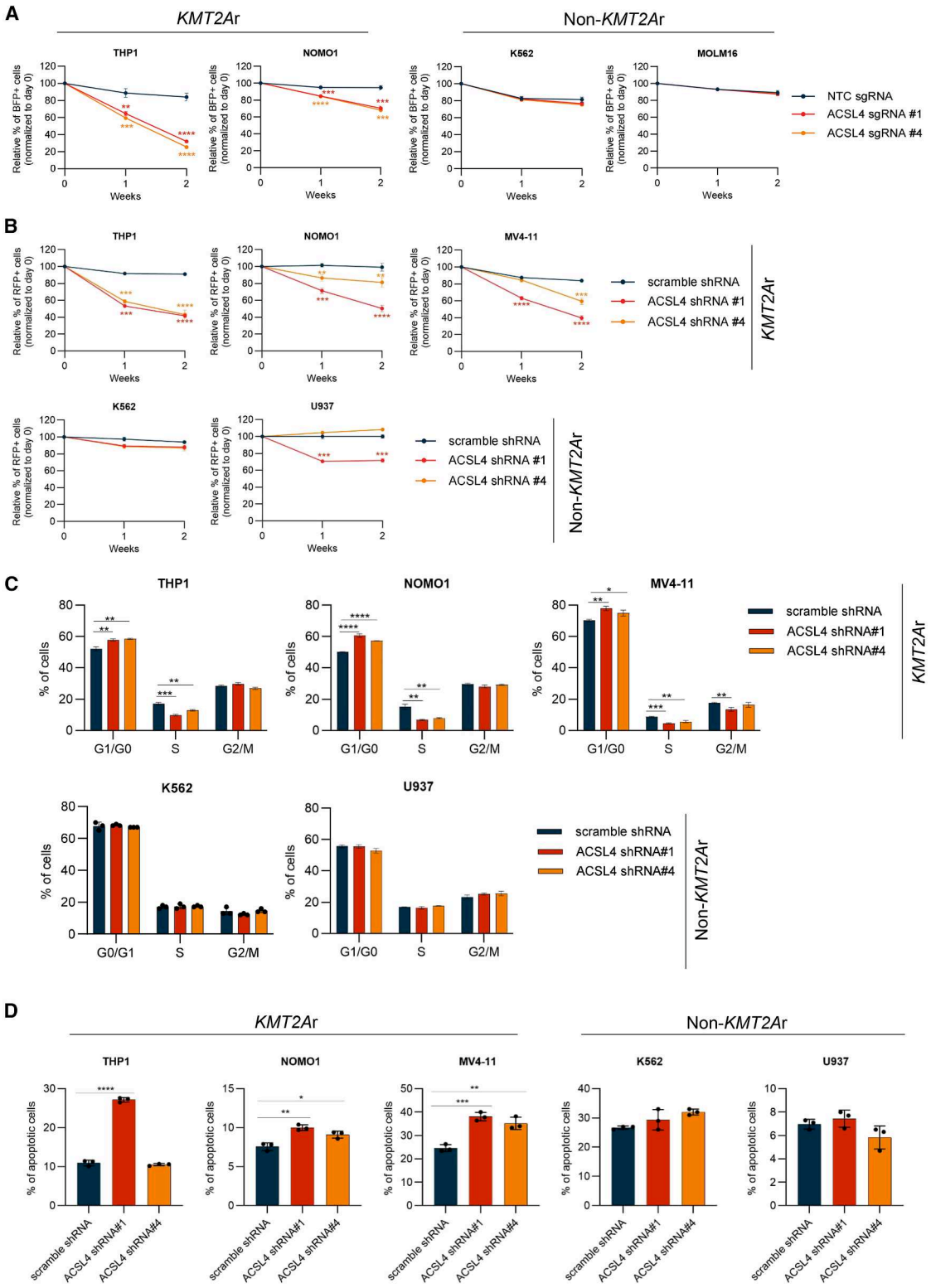

Figure 2. *ACSL4* knockdown reduces proliferation exclusively in *KMT2Ar* AML

(A) Flow cytometry-based competition assay of CRISPRi-induced *ACSL4* knockdown in *KMT2Ar* and non-*KMT2Ar* AML cell lines. The percentage of BFP+ cells represents the proportion of positively transduced cells harboring the sgRNA-BFP construct.

(legend continued on next page)

ACSL4-dependent compared to non-dependent cell lines (Figure S1D; Table S1D). Taken together, specifically *KMT2Ar* AML cell lines demonstrate a higher *ACSL4* dependency than non-*KMT2Ar* AML cell lines.

ACSL4 knockdown reduces proliferation exclusively in *KMT2Ar* AML

We next investigated the functional significance of *ACSL4* in *KMT2Ar* and non-*KMT2Ar* AML. Here, we utilized two cell lines representative of *KMT2Ar* AML (THP1 and NOMO1) and two cell lines representative of non-*KMT2Ar* AML (K562 and MOLM16), all four stably expressing dCas9-KRAB. We induced a CRISPR interference (CRISPRi)-based knockdown by transducing the cells with *ACSL4*-targeting or non-targeting single guide RNAs (sgRNAs), each co-expressing blue fluorescent protein (BFP). As a readout, we performed a flow cytometry-based competition assay, where the BFP signal represented the positively transduced cell population. The *KMT2Ar* cell lines revealed a decreased percentage of BFP+ cells over time when transduced with the *ACSL4*-targeting sgRNAs, whereas the percentage of BFP+ cells in the non-*KMT2Ar* cell lines remained constant over time (Figure 2A). To validate and extend these findings, we performed RNAi-based knockdowns across a broader panel of AML cell lines. Consistent with the CRISPRi results, *ACSL4* silencing by short hairpin RNAs (shRNAs) conferred a growth disadvantage in the *KMT2Ar* cell lines THP1, NOMO1, and MV4-11, but caused only a moderate reduction in non-*KMT2Ar* U937 cells with one of the two shRNAs and did not alter growth in non-*KMT2Ar* K562 cells (Figure 2B). Given that THP1 and NOMO1 cells harbor *KMT2A*::*MLLT3* rearrangements, whereas MV4-11 cells carry a *KMT2A*::*AFF1* fusion, the observed *ACSL4* dependency does not appear to be restricted to a single *KMT2Ar* subtype. Knockdown efficiency was confirmed by qPCR and western blot (Figures S2A–S2C).

To investigate the mechanism underlying the growth disadvantage observed in the competition assays upon *ACSL4* knockdown, we next analyzed cell cycle distribution and apoptosis. In the *KMT2Ar* cell lines THP1, NOMO1, and MV4-11, *ACSL4* knockdown, particularly with shRNA#1, led to an accumulation of cells in the G0/G1 phase of the cell cycle and a marked increase in apoptotic cells. In contrast, the non-*KMT2Ar* cell lines U937 and K562 showed no detectable changes in cell cycle distribution and apoptosis (Figures 2C and 2D). These results indicate that the reduced growth of *KMT2Ar* AML cells following *ACSL4* depletion is associated with G0/G1 arrest and enhanced apoptosis.

ACSL4 depletion impairs *ex vivo* growth and *in vivo* leukemic expansion in *KMT2Ar* AML models

To further validate *ACSL4* dependency and explore its functional significance in human patient-derived AML models, we performed colony-forming unit (CFU) assays. Two patient-derived xenograft (PDX) samples from individuals with *KMT2Ar* AML carrying distinct fusions PDX-388 (*KMT2A*::*MLLT4*) and PDX-393 (*KMT2A*::*MLLT10*), as well as a PDX sample from an individual with non-*KMT2Ar* AML (PDX-002) and peripheral blood mononuclear cells (PBMCs) from a healthy donor, were transduced with two independent *ACSL4*-targeting shRNAs or a scramble control. Transduction efficiency, as determined by red fluorescent protein (RFP) positivity, was approximately 60%–80% for PDX cells and ~30% for PBMCs, respectively, before plating. *ACSL4* knockdown efficiency of RFP+ purified cells was confirmed by qPCR (Figure S3A). The cells were plated in semisolid methylcellulose medium without antibiotic selection to assess clonogenic potential independent of selection pressure and to perform RFP+ vs. RFP− growth competition. After 2 weeks in semisolid culture, both *KMT2Ar* PDX samples exhibited a significantly lower number compared to the scramble control. In contrast, *ACSL4* knockdown in the non-*KMT2Ar* PDX or healthy PBMCs did not affect colony formation (Figures 3A, S3B, and S3C). Moreover, flow cytometric analysis of CFU-derived cells after 2 weeks revealed a decrease in RFP+ cells specifically in the *KMT2Ar* models, indicating that *ACSL4*-depleted (RFP+) leukemic cells exhibited a growth disadvantage compared to *ACSL4* WT RFP− cells (Figure 3B).

To extend these findings to an experimental mouse model of *KMT2Ar* AML, we next used the MLL-AF9 system, expressing the human fusion protein *KMT2A*::*MLLT3* in murine $Cd45^{+}$ leukocytes.[28] We designed shRNAs targeting murine *Acsl4* and stably transduced previously isolated Ly5.2 MLL-AF9 cells. For our *ex vivo* approach, we assessed the CFU capacity of MLL-AF9-*Acsl4* knockdown and scramble control cells within a semisolid medium assay. Here, we observed a significantly decreased colony number in *Acsl4* knockdown MLL-AF9 cells compared to the scramble control. Interestingly, in healthy bone marrow mononuclear cells (BMMCs), *Acsl4* knockdown with shRNA#1 led to an increase in colony formation, whereas shRNA#3 had little or no effect (Figures 3C, S3D, and S3E).

Next, for our *in vivo* approach, we transduced MLL-AF9 cells with either an *Acsl4* shRNA or a scramble control and transplanted the cells into Ly5.1 recipient mice (Figure 3D). As the maximum achievable transduction efficacy was around 60%–80% at the time of transplantation, we performed two complementary experimental approaches. First, we conducted an *in vivo* competition assay to track the contribution of RFP+ cells to leukemia development, similar to the previously mentioned CFU *in vitro* approach. Three weeks after transplantation, we performed peripheral blood analysis and compared the percentage of RFP+ cells to the initial transduction efficiency. We detected a significant decrease in RFP+ cells in the *Acsl4* knockdown group compared to the scramble control group, indicating a growth disadvantage and/or impaired engraftment of *Acsl4* knockdown

(B) Flow cytometry-based competition assay of RNAi-induced *ACSL4* knockdown in *KMT2Ar* and non-*KMT2Ar* AML cell lines. The percentage of RFP+ cells represents the proportion of positively transduced cells harboring the shRNA-RFP construct.
(C) Flow cytometry-based cell cycle analysis of *KMT2Ar* (THP1, NOMO1, and MV4-11) and non-*KMT2Ar* (K562 and U937) cells at 18 days post-transduction with shRNA against *ACSL4* or scramble control. Data represent the mean ± SD of three biological replicates.
(D) Percentage of Annexin V+ cells by flow cytometry in *KMT2Ar* (THP1, NOMO1, and MV4-11) and non-*KMT2Ar* (K562 and U939) cells at 18 days post-transduction with shRNA against *ACSL4* or scramble control. *p* value calculation based on a two-tailed Student's *t* test. $^{*}p < 0.05$, $^{**}p < 0.01$, $^{***}p < 0.001$, and $^{****}p < 0.0001$.

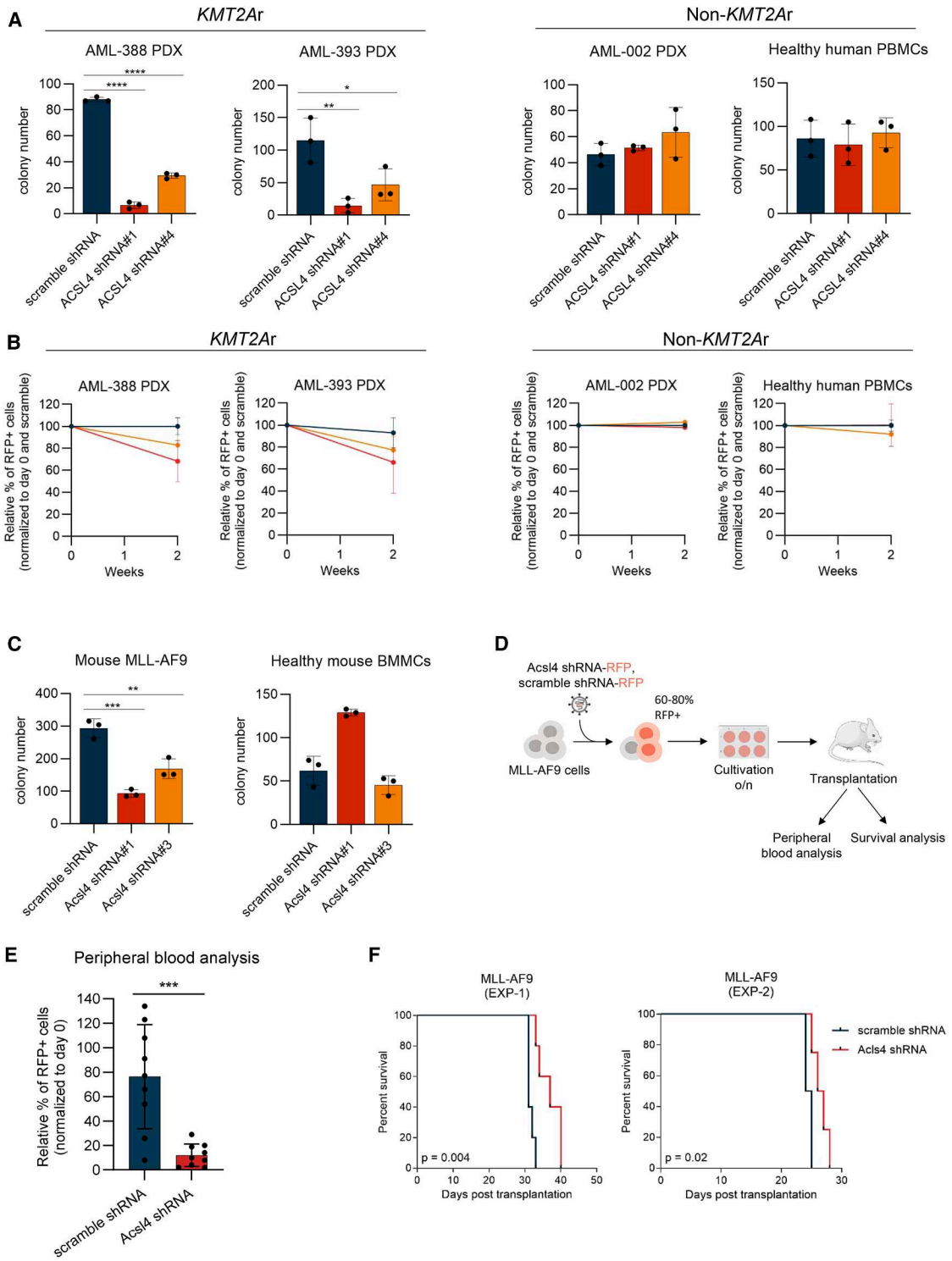

Figure 3. Knockdown of *ACSL4* impairs colony formation and leukemia progression in patient-derived and primary murine *KMT2Ar* AML models

(A) Quantification of colonies formed by AML PDX cells and healthy PBMCs seeded in methylcellulose (1×10^4 cells per well) for 14 days following *ACSL4* knockdown compared to the scramble control. Data represent the mean ± SD of three biological replicates. *p* value calculation based on a two-tailed Student's *t* test. $^*p < 0.05$, $^{**}p < 0.01$, and $^{****}p < 0.0001$.

(B) Flow cytometric quantification of the percentage of RFP+ cells seeded in CFU assays after 14 days.

(legend continued on next page)

cells *in vivo* (Figure 3E). Second, we assessed whether this reduction in RFP+ cells translated into differences in overall survival. Although non-transduced (RFP−) cells progressively outgrow the RFP+ knockdown cells in the *Acsl4* shRNA group and likely limit the detectable survival benefit, we found that mice receiving *Acsl4* knockdown MLL-AF9 cells showed a modest but reproducible extension in survival compared to controls across two independent transplantation experiments (Figure 3F).

Collectively, these findings demonstrate that *ACSL4* supports the *ex vivo* growth and *in vivo* expansion of *KMT2Ar* AML, and its depletion suppresses leukemic proliferation while sparing normal hematopoietic cells.

Disruption of *ACSL4* induces an upregulation of lipid metabolism pathways in *KMT2Ar* AML cells

We next investigated the consequences of *ACSL4* disruption on transcriptional changes and protein abundance using a multi-omics approach. Here, we introduced a CRISPRi-based *ACSL4* knockdown into NOMO1 dCas9-KRAB and K562 dCas9-KRAB cells, representing *KMT2Ar* and *KMT2A* WT cell lines, respectively, and isolated total RNA and protein for subsequent RNA sequencing (RNA-seq) and liquid chromatography-tandem mass spectrometry-based proteomics analysis (Figure 4A). We performed a differential gene expression (DGE) analysis on the transcriptomic data to identify up- and downregulated transcripts in both cell lines (Figure 4B; Tables S2A and S2B). In addition, we analyzed the proteome data to identify significantly up- and downregulated proteins (Figure 4C; Tables S3A and S3B). Next, we performed GSEA, which revealed an upregulation of pathways involved in lipid metabolism upon *ACSL4* knockdown at both the transcriptomic and the proteomic level in NOMO1 cells. Interestingly, we observed a downregulation of the same pathways in the *KMT2A* WT cell line K562 in both transcriptomics and proteomics data (Figure 4D). Furthermore, we uncovered additional pathways enriched in *KMT2Ar* cells following *ACSL4* depletion, including TNFα/NF-κB and mTORC1 signaling (Figure S4A). Together, these findings indicate that *ACSL4* loss reprograms both lipid metabolic and inflammatory signaling networks.

Next, we integrated the transcriptomic and proteomic data and generated overlaps of cell line-specific up- and downregulated transcripts and proteins. We identified 12 overlaps of upregulated transcripts and proteins in NOMO1 cells (Figure 4E), while there were no overlaps of upregulated transcripts and proteins in K562 cells and only a few overlaps of downregulated transcripts and proteins in both cell lines (Figures S4B and S4C). The 12 genes found in NOMO1 cells after *ACSL4* knockdown were used to generate a *KMT2A*-rearranged *ACSL4*-dependency signature (KRADS12) (Figures 4F, S4D, and S4E). To gain further insights into KRADS12-specific signaling pathways, we performed a functional enrichment analysis of the KRADS12 genes using g:profiler[29] and discovered that KRADS12 genes are predominantly involved in lipid metabolic pathways (Figure 4G). Taken together, our findings suggest that the knockdown of *ACSL4* induces an upregulation of lipid metabolism exclusively in *KMT2Ar* cells.

ACSL4 knockdown selectively alters lipid composition in *ACSL4*-dependent AML cells, and PUFA supplementation rescues growth defects in *KMT2Ar* models

Our transcriptomics and proteomics analyses revealed an upregulation of lipid metabolism pathways upon *ACSL4* knockdown in the *KMT2Ar* AML cell line NOMO1. Therefore, to further assess the changes in the lipid composition upon *ACSL4* knockdown, we performed an untargeted lipidome analysis comparing *ACSL4* knockdown to control cells in both NOMO1 and K562 cells (Figure S5A; Tables S4A and S4B). We observed significant systematic changes in cellular lipid composition upon *ACSL4* knockdown in NOMO1 cells but rather mild changes in K562 cells (Figures 5A and 5B). An analysis of differential lipid concentrations comparing *ACSL4* knockdown to control cells revealed a significant downregulation of 113 lipids in NOMO1 cells, while in K562 cells, only 2 lipids were downregulated (Figure 5C; Tables S4C and S4D). Next, we were interested in deregulated lipid classes upon *ACSL4* knockdown and detected a significant downregulation of ceramide (Cer), glycosylated ceramide (Hex2Cer), lysoalkylphosphatidylcholine (O-LPC), phosphatidylcholine (PC), phosphatidylserine (PS), and triacylglycerol (TG) lipids in NOMO1 compared to K562 cells (Figure S5B). Since ACSL4 activates PUFAs, we analyzed whether the strongly downregulated lipid classes PC and TG show differences in unsaturated FA composition. Indeed, PCs with 3, 4, 5, 6, 7, 9, and 10 double bonds were significantly downregulated upon *ACSL4* knockdown in NOMO1 cells compared to K562 cells. Interestingly, fully saturated PCs were also downregulated in NOMO1 compared to K562 cells upon *ACSL4* knockdown (Figure 5D). We observed similar findings in TG lipids. However, saturated TGs were not deregulated in NOMO1 compared to K562 cells upon *ACSL4* knockdown (Figure 5E). In NOMO1 cells, *ACSL4* knockdown led to a marked reduction in TGs and other lipid classes containing PUFAs, whereas K562 cells showed a slight increase in PUFA-containing lipids under the same conditions (Figure 5F). Collectively, the knockdown of *ACSL4* in *KMT2Ar* AML induces a strong downregulation of lipids, especially those with multiple double bonds. In contrast, the knockdown of *ACSL4* in *KMT2A* WT AML has only mild effects on lipid

(C) Quantification of counted colonies of MLL-AF9 expressing cells or healthy BMMCs, seeded in methylcellulose for 10 days (5×10^3 cells per well). Data represent the mean ± SD of three biological replicates. *p* value calculation based on a two-tailed Student's *t* test. $^{**}p < 0.01$ and $^{***}p < 0.001$.
(D) Graphical workflow overview of the generation of *Acsl4*-knockdown MLL-AF9 cells followed by transplantation into Ly5.1 mice.
(E) Peripheral blood analysis 3 weeks post-transplantation of Ly5.1 mice transplanted with either scramble or *Acsl4* shRNA-transduced MLL-AF9 cells from two pooled independent experiments. *p* value calculation based on two-tailed Student's *t* test ($^{***}p < 0.001$, $n = 9$ animals per group).
(F) Survival curve of Ly5.1 mice transplanted with MLL-AF9 cells transduced with either scramble or *Acsl4* shRNA, compiled from two independent experiments. In the first experiment, each group included 5 animals, and in the second, each group included 4 animals (total $n = 18$). Statistical significance was assessed by the log rank (Mantel-Cox) test.

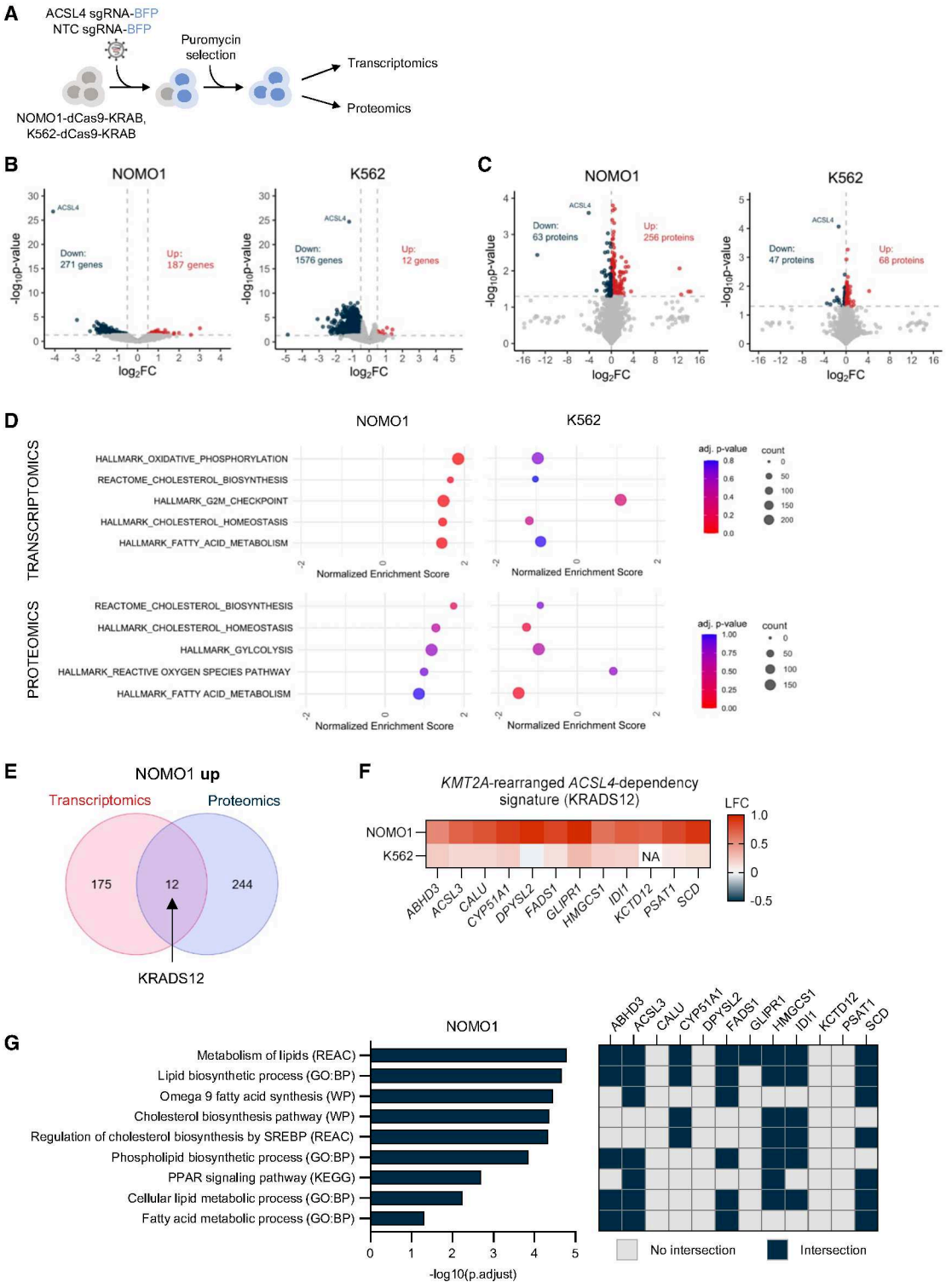

Figure 4. Disruption of *ACSL4* induces an upregulation of lipid metabolism pathways in *KMT2Ar* AML cells

(A) Graphical workflow overview of the generation of *ACSL4*-knockdown cell lines used for transcriptomics and proteomics.

(B) Volcano plots of differently expressed genes from RNA-seq analysis of NOMO1 dCas9-KRAB and K562 dCas9-KRAB cells expressing a non-targeting sgRNA or *ACSL4* sgRNA (n = 3 per group). Threshold of significantly depleted/enriched transcripts: p value < 0.05 and log fold change (LFC) </> 0.5.

(legend continued on next page)

composition. These findings further support our transcriptomics and proteomics results, where we observed an upregulation of lipid metabolism pathways in NOMO1 but not K562 cells upon *ACSL4* knockdown.

To determine whether the growth defect induced by *ACSL4* knockdown could be reversed, we performed rescue experiments using FA supplementation. Lipidomic profiling revealed a selective depletion of long-chain polyunsaturated lipid species (C20–C22) in NOMO1 but not in K562 cells following *ACSL4* knockdown. These depleted species included docosahexaenoic acid (DHA; 22:6), eicosapentaenoic acid (EPA; 20:5), arachidonic acid (AA; 20:4), adrenic acid (AdA; 22:4), and docosapentaenoic acid (DPA; 22:5). Consistent with previous reports identifying AA, EPA, DHA, and AdA as preferred ACSL4 substrates,[30] we formulated a defined cocktail containing these five PUFAs to restore the affected lipid pools. Following *ACSL4* knockdown, the culture medium was supplemented with this PUFA cocktail throughout the experiment. Interestingly, FA supplementation rescued the growth disadvantage of *ACSL4*-silenced cells in both *KMT2A*r models (Figure 5G). These findings indicate that the dependency on *ACSL4* in *KMT2A*r AML cells arises from impaired activation and incorporation of PUFAs into membrane phospholipids and that this metabolic vulnerability can be overcome by exogenous PUFA supply.

A high KRADS12 score is a predictor of poor outcome in patients with AML

Finally, we employed the KRADS12 signature to generate the KRADS12 score and evaluated the impact of the KRADS12 score on important clinical patient features using the two independent publicly available AML cohorts from the "The Cancer Genome Atlas" (TCGA)-LAML[4] (Figure 6A; Table S5A) and the Beat AML study.[31] For TCGA cohort, patients were divided into KRADS12^{high} and KRADS12^{low} groups using the median score as a cutoff, whereas for Beat AML, we compared the highest and lowest quartiles. In both cohorts, patients with KRADS12^{high} score had significantly shorter overall survival than patients with KRADS12^{low} score (TCGA n = 173, p = 0.011; Beat AML n = 649, p = 0.041 (Figure 6B). As a proof of concept, we stratified patients with AML from the Beat AML cohort into a *KMT2A*r or a *KMT2A* WT group. As expected, the *KMT2A*r downstream effector *HOXA9*, whose overexpression correlates with poor prognosis,[32–34] is significantly higher expressed in patients with *KMT2A*r than in those with *KMT2A* WT (Figure 6C). In addition, patients harboring a *KMT2A*r have a significantly higher KRADS12 score, compared to patients with *KMT2A* WT (Figure 6D). Finally, to understand the molecular differences between patients with KRADS12^{high} and KRADS12^{low}, we performed GSEA on the patient gene expression dataset of the TCGA-LAML cohort (Table S5B). Here, we identified various pathways associated with lipid metabolism as the top-enriched pathways, comparing patients with KRADS12^{high} to KRADS12^{low}. Further, *KMT2A* (*MLL*) signatures were among the top upregulated signatures in patients with KRADS12^{high}, supporting our previous findings (Figure 6E). In addition, patients with KRADS12^{high} exhibited consistent enrichment of hallmarks related to JAK-STAT, TNFα-NF-κB, and MTORC1 signaling, similar to our transcriptomics data from *KMT2A*r cells (Figures S4A and S6). Conversely, the cell cycle-related MYC_TARGETS signature was enriched in patients with KRADS12^{low}, indicating reduced MYC transcriptional activity in cases with KRADS12^{high} (Figure S6). This pattern aligns with the G0/G1 arrest observed upon *ACSL4* knockdown. Altogether, the KRADS12 score predicts patient outcome and correlates with an altered lipid metabolism, reduced proliferation, apoptosis, and inflammatory pathway activation characteristic of *ACSL4*-dependent *KMT2A*r AML.

DISCUSSION

In this study, we identified the lipid metabolic enzyme ACSL4 as a dependency of *KMT2A*r AML. We demonstrated that the genetic perturbation of *ACSL4* induces a growth arrest and apoptosis exclusively in *KMT2A*r but not in non-*KMT2A*r cell lines. This selective dependency was further validated in patient-derived AML models, where *ACSL4* silencing markedly reduced colony-forming capacity in two independent *KMT2A*r AML PDX samples carrying distinct fusions but had no effect in non-*KMT2A*r PDX or healthy PBMCs. Consistently, *Acsl4* knockdown also impaired leukemia maintenance in an MLL-AF9 mouse model, demonstrating a competitive disadvantage of *Acsl4*-deficient cells *in vivo*. Surprisingly, ACSL4 has been mostly described as an inducer of ferroptosis, thus having a rather tumor-suppressive function.[35–37] Ferroptosis is a type of regulated cell death characterized by an iron-dependent lipid peroxidation of PUFAs in the cell membrane.[38] Increased synthesis of PUFAs, which is facilitated by ACSL4, leads to increased ferroptosis.[37] In our study, we observed a decreased proliferation upon *ACSL4* knockdown, which is inconsistent with the previously reported role of *ACSL4* as a ferroptosis inducer. Therefore, we hypothesize that the observed effects upon *ACSL4* knockdown in our experimental setup are ferroptosis-independent. However, experiments testing specific ferroptosis markers are necessary to exclude ferroptosis as the underlying process of decreased proliferation.

(C) Volcano plots of differently expressed proteins from proteomics analysis of NOMO1 dCas9-KRAB and K562 dCas9-KRAB cells expressing a non-targeting sgRNA or *ACSL4* sgRNA (n = 4 per group). Threshold of significantly enriched/depleted proteins: p value < 0.05.
(D) GSEA analysis of the RNA-seq and proteomics data comparing the non-targeting sgRNA to the *ACSL4* sgRNA in NOMO1 and K562 cells. Bubble color represents the adjusted p value (false discovery rate q value), the bubble size represents the number of genes per gene set.
(E) Venn diagram of upregulated transcripts and proteins in NOMO1 cells. Overlapping 12 genes were used to generate a *KMT2A*r *ACSL4*-dependency signature.
(F) Heatmap of 12 overlapping genes and proteins in (E), which were used to generate the KRADS12 signature. Data represent RNA-seq data. Color indicates the LFC of transcript expression.
(G) Functional enrichment analysis of the KRADS12 genes by g:profiler indicates an association with various lipid metabolism pathways. Right: illustration of the KRADS12 genes included in each annotated pathway.

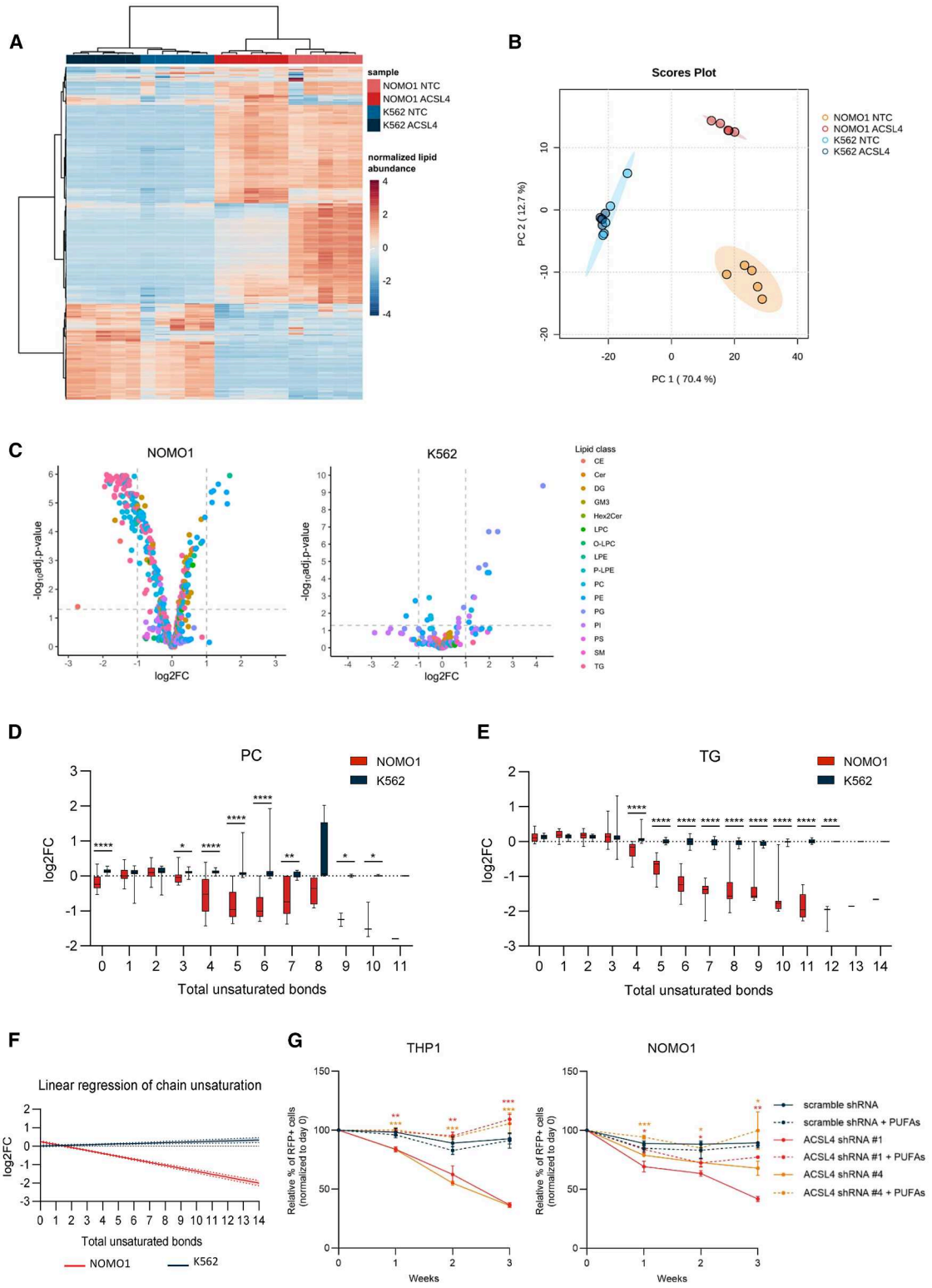

Figure 5. *ACSL4* knockdown alters lipid composition, and PUFA supplementation rescues growth in *KMT2A*r AML cells

(A) Hierarchical clustering heatmap of lipids quantified in NOMO1 and K562 cells expressing dCas9-KRAB with either a non-targeting control (NTC) or an *ACSL4*-targeting sgRNA (n = 5 biological replicates per group). Comparisons were performed between *ACSL4* knockdown and matched controls within each cell line.

(legend continued on next page)

We performed a multi-omics approach, including transcriptomics, proteomics, and lipidomics, to uncover differences in *ACSL4*-dependent vs. non-dependent AML upon *ACSL4* knockdown. Interestingly, this approach revealed a strong upregulation of pathways involved in lipid metabolism exclusively in *KMT2A*r and *ACSL4*-dependent AML, whereas *KMT2A* WT cells showed a downregulation of the same pathways upon *ACSL4* knockdown. Among the most upregulated pathways in *KMT2A*r AML were "FA metabolism" and "cholesterol metabolism." In addition, pathways associated with *ACSL4* inhibition in this AML subtype highlighted "omega-9 FA synthesis," "cholesterol biosynthesis," and "peroxisome proliferator-activated receptor (PPAR) signaling pathway" as the most enriched pathways. The upregulation of these cellular cascades may result from the activation of alternative pathways to produce sufficient amounts of activated FAs as a form of intracellular compensation. Interestingly, our lipidomics data reveal a decreased abundance of many lipids upon *ACSL4* knockdown in NOMO1 cells, especially of those with polyunsaturated acyl chains. This observation could indicate that the upregulation of lipid metabolic pathways is insufficient to compensate for *ACSL4* disruption in NOMO1 cells, thus not being sufficient as a compensatory mechanism to keep *KMT2A*r AML aggressiveness. Consistent with this, supplementation with exogenous PUFAs rescued the growth defect, confirming that impaired PUFA activation, rather than global lipid depletion, underlies the *ACSL4* dependency in *KMT2A*r AML.

Within our work, we defined a gene expression signature that is closely associated with the *ACSL4* knockdown in *KMT2A*r AML, which we named KRADS12. Gene signatures have a strong potential to serve as prognostic and predictive tools in AML, and various examples for individual cell types or biomarkers have been proposed.[39–41] A key member within the KRADS12 signature is ACSL3, an isoenzyme of the ACSL family that prefers monounsaturated fatty acids as substrates. The transcriptional activator PPARδ interacts with the PPAR response element within the *ACSL3* promoter, thereby upregulating *ACSL3* transcription.[42] Substrates for the PPARs include various FAs, and it has been reported that PPARs could serve as sensors of FA levels.[43] Thus, we speculate that the upregulation of PPARs upon *ACSL4* knockdown could serve as a compensatory mechanism to induce an upregulation of *ACSL3*, substituting *ACSL4*. Increased levels of PPARδ have also been reported in the context of chronic lymphocytic leukemia (CLL), where it protected CLL cells by upregulating antioxidant genes and increasing energy production through different metabolic processes.[44] These findings highlight the involvement of lipid metabolic processes in leukemogenesis and are consistent with our findings. In the BEAT AML cohort, the KRADS12 score showed a less pronounced prognostic effect than in TCGA, likely reflecting the cohort's greater biological and clinical heterogeneity, including differences in treatment, disease stage, and sample composition. Still, patients in the highest KRADS12 quartile showed the poorest survival, indicating that KRADS12 is a valuable biomarker for identifying *KMT2A*r with distinct metabolic dependencies.

Besides ACSL4, other enzymes involved in fatty acid metabolism have been reported as tumor promoters in a plethora of leukemia subtypes, such as very long chain acyl-CoA dehydrogenase (VLCAD) and FA desaturase 1 (FADS1) in AML[9,18] and very long chain FA elongase 1 (ELOVL1) in infant MLL-AF4-driven acute lymphoblastic leukemia (ALL).[45] Taken together, our and other studies suggest that FA metabolism is essential for leukemia cells and that enzymes involved in FA metabolism provide promising targets for anti-leukemic treatment.

In this study, we identified *ACSL4* as a vulnerability specifically in *KMT2A*r AML. Although the precise molecular mechanisms underlying this unique *ACSL4* dependency in *KMT2A*r AML remain to be elucidated, our findings suggest a distinctive reliance on exogenous and/or ACSL4-activated PUFAs in this aggressive leukemia subtype. Our GSEA analysis upon *ACSL4* knockdown revealed enrichment of lipid metabolism-related (cholesterol homeostasis and FA metabolism) and cytokine signaling pathways (TNFα/NF-κB and mTORC1) specifically in *KMT2A*r cells. Consistent with these findings, other studies have also reported a specific dependency of *KMT2A*r AML on FA metabolism: the consumption of a high-fat diet in a *KMT2A*r knockin mouse model accelerated the risk of developing AML by activating FLT3 and the JAK/STAT signaling pathway.[46] Additionally, the pharmacological inhibition of JMJD1C, an epigenetic regulator of various lipid metabolic enzymes, selectively induced apoptosis in *KMT2A*r AML cell lines.[47] Notably, both NF-κB and mTORC1 pathways have been implicated in maintaining leukemic self-renewal and

(B) Principal component analysis (PCA) scores plot of lipids quantified in NOMO1 and K562 cells expressing dCas9-KRAB and a non-targeting or *ACSL4*-targeting sgRNA ($n = 5$ replicates per group).

(C) Volcano plots of differentially abundant lipids in NOMO1 dCas9-KRAB and K562 dCas9-KRAB cells expressing a non-targeting sgRNA or *ACSL4* sgRNA ($n = 5$ per group). Threshold of significantly depleted/enriched lipids: p value < 0.05 and LFC </> 1. Lipid classes are depicted in different colors (cholesteryl esters [CE], ceramides [Cer], diglyceride [DG], ganglioside GM3 [GM3], doubly hexosylated ceramide [Hex2Cer], lysophosphatidylcholine [LPC], lysoalkylphosphatidylcholine [O-LPC], lysophosphatidylethanolamine [LPE], lysoalkenylphosphatidylethanolamine [P-LPE], phosphatidylcholine [PC], phosphatidylethanolamine [PE], phosphatidylglycerol [PG], phosphatidylinositol [PI], phosphatidylserine [PS], sphingomyelin [SM], and triacylglycerol [TG].

(D) Total number of unsaturated bonds in PC lipids comparing NOMO1 dCas9-KRAB and K562 dCas9-KRAB cells upon *ACSL4* knockdown. y axis represents log2 fold change (FC) of the differential analysis of lipid abundance.

(E) Total number of unsaturated bonds in TG lipids comparing NOMO1 dCas9-KRAB and K562 dCas9-KRAB cells upon *ACSL4* knockdown. y axis represents log2FC of the differential analysis of lipid abundance.

(F) Linear regression analysis of the number of total unsaturated bonds among all lipids upon *ACSL4* knockdown in NOMO1 dCas9-KRAB and K562 dCas9-KRAB cells. y axis represents log2FC of the differential analysis of lipid abundance.

(G) Rescue experiment in THP1 and NOMO1 (*KMT2A*r) AML cells. Following *ACSL4* or scramble knockdown, cells were supplemented with a cocktail of selected PUFAs (DHA, EPA, AA, AdA, and DPA), and the percentage of RFP+ cells was measured by flow cytometry in a competition assay over time. p value calculation based on a two-tailed Student's t test. $^{*}p < 0.05$, $^{**}p < 0.01$, $^{***}p < 0.001$, and $^{****}p < 0.0001$.

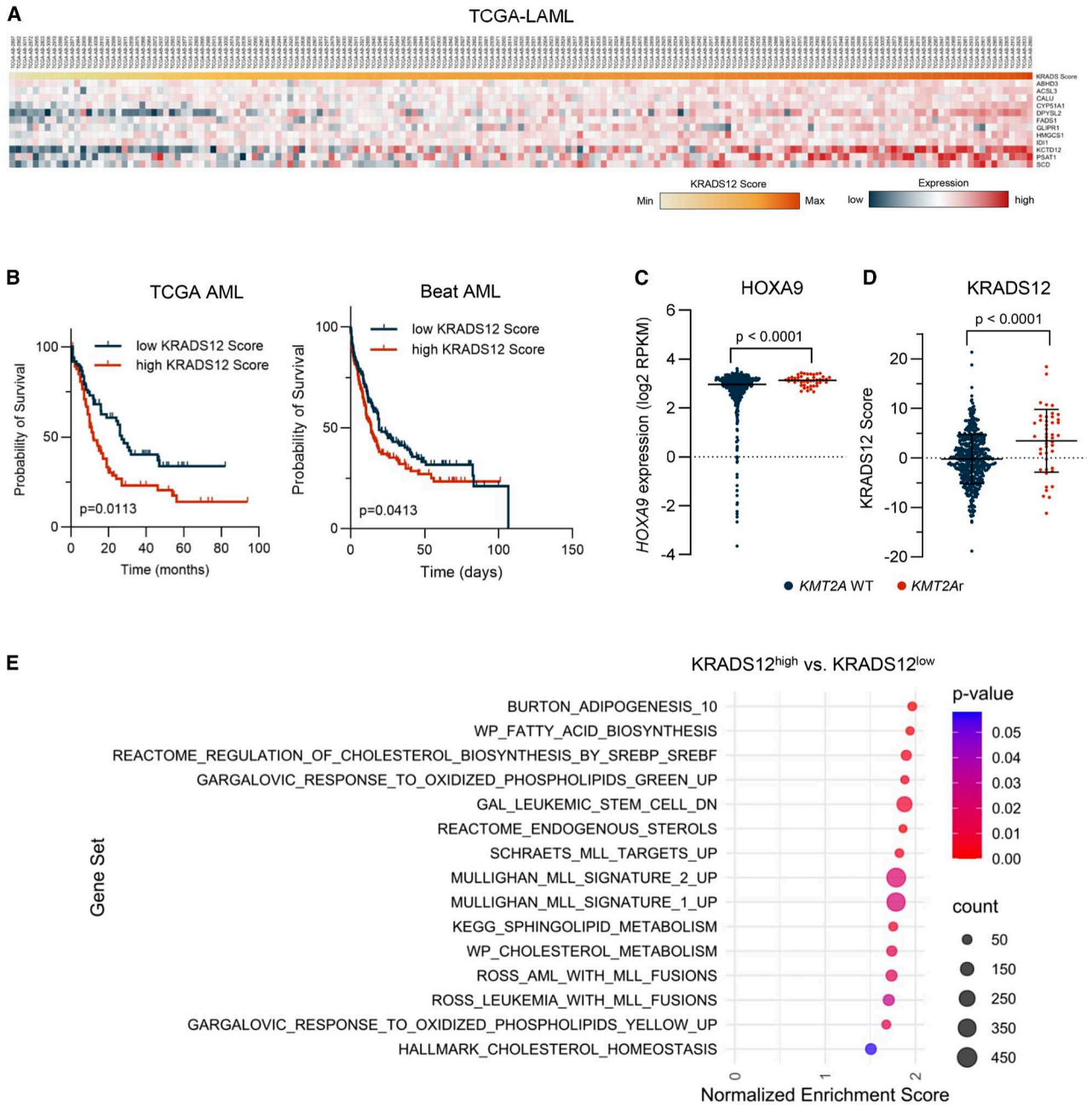

Figure 6. A high KRADS12 score is a predictor of poor outcome in patients with AML

(A) Heatmap of patients with LAML in TCGA cohort and the expression of all KRADS12 genes per patient ordered according to increased expression of the KRADS12 signature from left (KRADS12^{low}) to right (KRADS12^{high}).

(B) Analysis of the impact of the KRADS12 score on patient survival within the TCGA-LAML cohort and Beat AML cohort. Patients in TCGA-LAML were stratified into *KRADS12^{low}* and *KRADS12^{high}* groups based on the median KRADS12 score, whereas in the Beat AML cohort, patients in the lowest and highest quartiles were compared. *p* value calculation based on Gehan-Breslow-Wilcoxon test.

(C and D) Comparison of *HOXA9* gene expression (C) and KRADS12 score (D) between patients with *KMT2A* WT ($n = 525$) and *KMT2Ar* ($n = 45$) AML in the Beat AML cohort. *p* value calculation based on a two-tailed Mann-Whitney test.

(E) GSEA comparing people with LAML from TCGA cohort with KRADS^{high} ($n = 86$) vs. KRADS12^{low} ($n = 87$). The bubble color represents the *p* value, and the bubble size indicates the number of genes per gene set.

stress resilience downstream of *KMT2A* fusion proteins,[48–50] suggesting that *ACSL4* loss may elicit compensatory activation of lipid and inflammatory signaling exclusively in *KMT2A*r AML. These findings indicate a mechanistic link between *ACSL4*-dependent lipid metabolism and *KMT2A*-driven transcriptional programs.

Further studies are needed to prove *ACSL4* as a therapeutic target in *KMT2A*r AML, for instance, by pharmacological inhibition of the enzymatic activity of ACSL4. Interestingly, there are preclinical compounds available that interfere with the ACSL4 cascade. For instance, the pan-ACSL inhibitor triacsin C has been reported to reduce the growth of non-small-cell lung cancer in combination with chemotherapy.[51] In addition, the inhibitor PRGL493 is highly specific for ACSL4 and showed anti-proliferative effects in breast and prostate cancer cell lines and animal models.[20] Exploiting FA metabolism targets as treatment strategies for AML has been shown to be very effective in previous studies: venetoclax with azacytidine (ven/aza)-resistant leukemic stem cells (LSCs) of patients with AML have an increased expression of PUFAs and increased metabolites involved in FA transport into the mitochondria. Inhibition of the enzyme very-long-chain acyl-CoA dehydrogenase (ACADVL) restored the ven/aza sensitivity of LSCs.[52] Furthermore, the rate-limiting enzyme for *de novo* FA synthesis, ACACA, is overexpressed in *IDH1*-mutated AML, and a lipid-free diet in *IDH1*-mutant AMLs transplanted into NSG mice showed a significantly decreased engraftment compared to the normal diet control group.[53] Overall, biomarkers to predict response to FA metabolism-targeting therapy, as well as selective inhibitors with high specificity, are highly needed to exploit FA metabolism as a potential therapeutic strategy in AML. In conclusion, we present in this study the FA metabolism gene *ACSL4* as a selective therapeutic target in the aggressive *KMT2A*r AML subtype.

Limitations of the study

While our study provides comprehensive functional and multi-omics evidence identifying *ACSL4* as a selective metabolic vulnerability in *KMT2A*r-AML, several limitations should be acknowledged. The mechanistic insights, although supported by integrated transcriptomic, proteomic, and lipidomic analyses, were derived from a limited number of representative models and may not fully capture the genetic and metabolic heterogeneity across distinct *KMT2A*r AML subtypes or co-occurring mutations. Similarly, the KRADS12 signature was derived primarily from transcriptomic and proteomic data of the NOMO1 cell line, which, while representative of *KMT2A*r AML, may not fully capture the biological diversity of patient-derived leukemias. Finally, although we observed ferroptosis-independent effects upon *ACSL4* loss, we did not directly assess ferroptosis markers or reactive oxygen species levels, which limits the definitive conclusions about the mode of cell death. Future investigations should delineate the molecular mechanisms by which ACSL4 regulates lipid metabolism in *KMT2A*r leukemia, explore combinatorial therapeutic strategies targeting this metabolic axis, and validate the KRADS12 signature as a predictive biomarker in clinically annotated patient cohorts.

RESOURCE AVAILABILITY

Lead contact

Further information and requests for resources and reagents should be directed to and will be fulfilled by the lead contact, Alexander A. Wurm (alexander.wurm@nct-dresden.de).

Materials availability

All materials generated in this study are available from the lead contact.

Data and code availability

- RNA-seq data have been deposited in the Gene Expression Omnibus (GEO) repository with the accession number GEO: GSE274462 and are publicly available at https://www.ncbi.nlm.nih.gov/geo/query/acc.cgi?acc=GSE274462. The mass spectrometry proteomics data have been deposited to the ProteomeXchange Consortium via the PRIDE partner repository with the dataset identifier PRIDE: PXD072756 (https://www.ebi.ac.uk/pride/archive/projects/PXD072756). All datasets are listed in the key resources table. Processed dependency, expression, proteomics, and lipidomics data files are listed in the supplemental information section.
- This paper does not report original code.
- Any additional information required to reanalyze the data reported in this paper is available from the lead contact upon request.

ACKNOWLEDGMENTS

The authors thank the members of the Department of Translational Medical Oncology (TMO), the Patient-derived Tumor Model Unit (PMU), the Core Unit for Molecular Tumor Diagnostics (CMTD) at the NCT/UCC Dresden, and the Dresden International Graduate School for Interdisciplinary Life Sciences (DIGS-ILS) for constant support. This work was supported by grants from DFG (German Research Foundation, WU977/2-1), Deutsche Krebshilfe (70114086), and TU Dresden (MeDDrive) to A.A.W.; by Deutsche Krebshilfe (Mildred-Scheel program) to M. Bill and A.A.W.; and by TU Dresden (MeDDrive) and Stiftung Hochschulmedizin to M. Bill. Further, the study was partially supported by the Czech Health Research Agency (grant NU22-07-00087) to M.A.-J. and by the National Institute for Cancer Research (program EXCELES, project no. LX22NPO5102)—funded by the European Union - Next Generation EU. Work in the Fedorova lab is supported by ''Sonderzuweisung zur Unterstützung profilbestimmender Struktureinheiten'' by the SMWK to TUD, TG70 by Sächsische Aufbaubank and SMWK (the measure is co-financed with tax funds on the basis of the budget passed by the Saxon state parliament, to M.F.), Deutsche Forschungsgemeinschaft (FE 1236/5-1, FE 1236/8-1 to M.F.), and Bundesministerium für Bildung und Forschung (01EJ2205A, FERROPath to M.F.).

AUTHOR CONTRIBUTIONS

Performed experiments, S.S., E.R., L.S.-H., S.B., V.K., S.K., M.F., N.K., Z.N., and D.H.; conceived and designed the study, S.S., M. Bill, and A.A.W.; conceived and designed revision, E.R., M. Bill, and A.A.W.; analyzed data, S.S., E.R., L.S.-H., S.B., V.K., S.K., M.F., N.K., Z.N., and D.H.; designed and performed *in vivo* experiments, M.S. and M.A.-J.; provided infrastructure and contributed to the study strategy, I.J., D.M.S., C.R.B., M. Bornhäuser, and H.G.; wrote the manuscript, E.R., S.S., M. Bill, and A.A.W.; supervised the work, M. Bill and A.A.W.; read, edited, and approved the final manuscript, all authors.

DECLARATION OF INTERESTS

The authors declare no competing interests.

DECLARATION OF GENERATIVE AI AND AI-ASSISTED TECHNOLOGIES IN THE WRITING PROCESS

The authors used ChatGPT, developed by OpenAI, to provide initial R code templates used in this study and for language editing assistance in this

manuscript. ChatGPT was solely utilized for language proofreading purposes and did not contribute to or influence any intellectual content within the manuscript.

STAR★METHODS

Detailed methods are provided in the online version of this paper and include the following:

- KEY RESOURCES TABLE
- EXPERIMENTAL MODEL AND STUDY PARTICIPANT DETAILS
  - Animal studies
  - Cell lines
  - Patient-derived xenograft (PDX)
- METHOD DETAILS
  - Cancer dependency map (DepMap)
  - Gene Set Enrichment Analysis (GSEA) of DepMap data
  - sgRNA and shRNA cloning
  - Production of lentiviral and retroviral particles
  - CRISPR interference
  - RNA interference
  - Flow cytometry-based competition assay
  - Apoptosis and cell cycle analysis
  - Colony-forming unit (CFU) assay
  - MLL-AF9 cell transduction, transplantation, and peripheral blood analysis
  - Organ collection and flow cytometry analysis
  - Protein isolation and western blot
  - RNA isolation, cDNA synthesis, and quantitative real-time PCR (qPCR)
  - Library preparation for RNA sequencing and data analysis
  - Proteomics
  - Lipidomics
  - Analysis of external datasets
- QUANTIFICATION AND STATISTICAL ANALYSIS

SUPPLEMENTAL INFORMATION

Supplemental information can be found online at https://doi.org/10.1016/j.celrep.2026.117010.

Received: November 5, 2024
Revised: November 4, 2025
Accepted: January 22, 2026
Published: February 18, 2026

REFERENCES

1. Döhner, H., Weisdorf, D.J., and Bloomfield, C.D. (2015). Acute Myeloid Leukemia. N. Engl. J. Med. https://doi.org/10.1002/9781118010136.ch5.
2. Fruchtman, H., Avigan, Z.M., Waksal, J.A., Brennan, N., and Mascarenhas, J.O. (2024). Management of isocitrate dehydrogenase 1/2 mutated acute myeloid leukemia. Leukemia *38*, 927–935. https://doi.org/10.1038/s41375-024-02246-2.
3. Smith, C.C. (2019). The growing landscape of FLT3 inhibition in AML. Hematology *2019*, 539–547. https://doi.org/10.1182/hematology.2019000058.
4. (2013). Genomic and Epigenomic Landscapes of Adult De Novo Acute Myeloid Leukemia. N. Engl. J. Med. *368*, 2059–2074. https://doi.org/10.1056/NEJMoa1301689.
5. Döhner, H., Wei, A.H., Appelbaum, F.R., Craddock, C., DiNardo, C.D., Dombret, H., Ebert, B.L., Fenaux, P., Godley, L.A., Hasserjian, R.P., et al. (2022). Diagnosis and management of AML in adults: 2022 recommendations from an international expert panel on behalf of the ELN. Blood *140*, 1345–1377. https://doi.org/10.1182/blood.2022016867.
6. Biondi, A., Cimino, G., Pieters, R., and Pui, C.H. (2000). Biological and therapeutic aspects of infant leukemia. Blood *96*, 24–33.
7. Issa, G.C., Ravandi, F., DiNardo, C.D., Jabbour, E., Kantarjian, H.M., and Andreeff, M. (2021). Therapeutic implications of menin inhibition in acute leukemias. Leukemia *35*, 2482–2495. https://doi.org/10.1038/s41375-021-01309-y.
8. Yu, B.D., Hess, J.L., Horning, S.E., Brown, G.A., and Korsmeyer, S.J. (1995). Altered Hox expression and segmental identity in Mll-mutant mice. Nature *378*, 505–508. https://doi.org/10.1038/378505a0.
9. Tcheng, M., Roma, A., Ahmed, N., Smith, R.W., Jayanth, P., Minden, M.D., Schimmer, A.D., Hess, D.A., Hope, K., Rea, K.A., et al. (2021). Very long chain fatty acid metabolism is required in acute myeloid leukemia. Blood *137*, 3518–3532. https://doi.org/10.1182/blood.2020008551.
10. Chen, M., Tao, Y., Yue, P., Guo, F., and Yan, X. (2022). Construction and validation of a fatty acid metabolism risk signature for predicting prognosis in acute myeloid leukemia. BMC Genom. Data *23*, 85. https://doi.org/10.1186/s12863-022-01099-x.
11. Carracedo, A., Cantley, L.C., and Pandolfi, P.P. (2013). Cancer metabolism: fatty acid oxidation in the limelight. Nat. Rev. Cancer *13*, 227–232. https://doi.org/10.1038/nrc3483.
12. Samudio, I., Harmancey, R., Fiegl, M., Kantarjian, H., Konopleva, M., Korchin, B., Kaluarachchi, K., Bornmann, W., Duvvuri, S., Taegtmeyer, H., and Andreeff, M. (2010). Pharmacologic inhibition of fatty acid oxidation sensitizes human leukemia cells to apoptosis induction. J. Clin. Investig. *120*, 142–156. https://doi.org/10.1172/JCI38942.
13. Quan, J., Bode, A.M., and Luo, X. (2021). ACSL family: The regulatory mechanisms and therapeutic implications in cancer. Eur. J. Pharmacol. *909*, 174397. https://doi.org/10.1016/j.ejphar.2021.174397.
14. Harayama, T., and Shimizu, T. (2020). Roles of polyunsaturated fatty acids, from mediators to membranes. J. Lipid Res. *61*, 1150–1160. https://doi.org/10.1194/jlr.R120000800.
15. Van Meer, G., Voelker, D.R., and Feigenson, G.W. (2008). Membrane lipids: where they are and how they behave. Nat. Rev. Mol. Cell Biol. *9*, 112–124. https://doi.org/10.1038/nrm2330.
16. Kar, A., Ghosh, P., Patra, P., Chini, D.S., Nath, A.K., Saha, J.K., and Chandra Patra, B. (2023). Omega-3 fatty acids mediated Cellular signaling and its regulation in Human Health. Clin. Nutr. Open Sci. *52*, 72–86. https://doi.org/10.1016/j.nutos.2023.10.004.
17. Scott, J.S., Nassar, Z.D., Swinnen, J.V., and Butler, L.M. (2022). Monounsaturated Fatty Acids: Key Regulators of Cell Viability and Intracellular Signaling in Cancer. Mol. Cancer Res. *20*, 1354–1364. https://doi.org/10.1158/1541-7786.MCR-21-1069.
18. Kanefsky, J., Basse, M., Sokei, J., Di Martino, O., Valin, L., Jaspers, Y., Martinez, E., Huhn, J., Di Marcantonio, D., Magee, J.A., et al. (2024). Disruption of polyunsaturated fatty acid biosynthesis drives STING-dependent acute myeloid leukemia cell maturation and death. J. Biol. Chem. *300*, 107214. https://doi.org/10.1016/j.jbc.2024.107214.
19. Gupta, A., Das, D., and Taneja, R. (2024). Targeting Dysregulated Lipid Metabolism in Cancer with Pharmacological Inhibitors. Cancers *16*, 1313. https://doi.org/10.3390/cancers16071313.
20. Castillo, A.F., Orlando, U.D., Maloberti, P.M., Prada, J.G., Dattilo, M.A., Solano, A.R., Bigi, M.M., Ríos Medrano, M.A., Torres, M.T., Indo, S., et al. (2021). New inhibitor targeting Acyl-CoA synthetase 4 reduces breast and prostate tumor growth, therapeutic resistance and steroidogenesis. Cell. Mol. Life Sci. *78*, 2893–2910. https://doi.org/10.1007/s00018-020-03679-5.
21. Sánchez-Martínez, R., Cruz-Gil, S., Gómez de Cedrón, M., Álvarez-Fernández, M., Vargas, T., Molina, S., García, B., Herranz, J., Moreno-Rubio, J., Reglero, G., et al. (2015). A link between lipid metabolism and epithelial-mesenchymal transition provides a target for colon cancer therapy. Oncotarget *6*, 38719–38736. https://doi.org/10.18632/oncotarget.5340.

22. Ye, X., Zhang, Y., Wang, X., Li, Y., and Gao, Y. (2016). Tumor-suppressive functions of long-chain acyl-CoA synthetase 4 in gastric cancer: Tumor-Suppressive Functions of ACSL4. IUBMB Life *68*, 320–327. https://doi.org/10.1002/iub.1486.

23. Zhang, Y., Li, S., Li, F., Lv, C., and Yang, Q.K. (2021). High-fat diet impairs ferroptosis and promotes cancer invasiveness via downregulating tumor suppressor ACSL4 in lung adenocarcinoma. Biol. Direct *16*, 10. https://doi.org/10.1186/s13062-021-00294-7.

24. Kao, Y.-R., Chen, J., Kumari, R., Ng, A., Zintiridou, A., Tatiparthy, M., Ma, Y., Aivalioti, M.M., Moulik, D., Sundaravel, S., et al. (2024). An iron rheostat controls hematopoietic stem cell fate. Cell Stem Cell *31*, 378–397.e12. https://doi.org/10.1016/j.stem.2024.01.011.

25. Tsherniak, A., Vazquez, F., Montgomery, P.G., Weir, B.A., Kryukov, G., Cowley, G.S., Gill, S., Harrington, W.F., Pantel, S., Krill-Burger, J.M., et al. (2017). Defining a Cancer Dependency Map. Cell *170*, 564–576.e16. https://doi.org/10.1016/j.cell.2017.06.010.

26. Tzelepis, K., Koike-Yusa, H., De Braekeleer, E., Li, Y., Metzakopian, E., Dovey, O.M., Mupo, A., Grinkevich, V., Li, M., Mazan, M., et al. (2016). A CRISPR Dropout Screen Identifies Genetic Vulnerabilities and Therapeutic Targets in Acute Myeloid Leukemia. Cell Rep. *17*, 1193–1205. https://doi.org/10.1016/j.celrep.2016.09.079.

27. Yamauchi, T., Masuda, T., Canver, M.C., Seiler, M., Semba, Y., Shboul, M., Al-Raqad, M., Maeda, M., Schoonenberg, V.A.C., Cole, M.A., et al. (2018). Genome-wide CRISPR-Cas9 Screen Identifies Leukemia-Specific Dependence on a Pre-mRNA Metabolic Pathway Regulated by DCPS. Cancer Cell *33*, 386–400.e5. https://doi.org/10.1016/j.ccell.2018.01.012.

28. Krivtsov, A.V., Twomey, D., Feng, Z., Stubbs, M.C., Wang, Y., Faber, J., Levine, J.E., Wang, J., Hahn, W.C., Gilliland, D.G., et al. (2006). Transformation from committed progenitor to leukaemia stem cell initiated by MLL–AF9. Nature *442*, 818–822. https://doi.org/10.1038/nature04980.

29. Kolberg, L., Raudvere, U., Kuzmin, I., Adler, P., Vilo, J., and Peterson, H. (2023). g:Profiler—interoperable web service for functional enrichment analysis and gene identifier mapping (2023 update). Nucleic Acids Res. *51*, W207–W212. https://doi.org/10.1093/nar/gkad347.

30. Shimbara-Matsubayashi, S., Kuwata, H., Tanaka, N., Kato, M., and Hara, S. (2019). Analysis on the Substrate Specificity of Recombinant Human Acyl-CoA Synthetase ACSL4 Variants. Biol. Pharm. Bull. *42*, 850–855. https://doi.org/10.1248/bpb.b19-00085.

31. Bottomly, D., Long, N., Schultz, A.R., Kurtz, S.E., Tognon, C.E., Johnson, K., Abel, M., Agarwal, A., Avaylon, S., Benton, E., et al. (2022). Integrative analysis of drug response and clinical outcome in acute myeloid leukemia. Cancer Cell *40*, 850–864.e9. https://doi.org/10.1016/j.ccell.2022.07.002.

32. Zeisig, B.B., Milne, T., García-Cuéllar, M.-P., Schreiner, S., Martin, M.-E., Fuchs, U., Borkhardt, A., Chanda, S.K., Walker, J., Soden, R., et al. (2004). *Hoxa9* and *Meis1* Are Key Targets for MLL-ENL-Mediated Cellular Immortalization. Mol. Cell Biol. *24*, 617–628. https://doi.org/10.1128/MCB.24.2.617-628.2004.

33. Armstrong, S.A., Staunton, J.E., Silverman, L.B., Pieters, R., Den Boer, M.L., Minden, M.D., Sallan, S.E., Lander, E.S., Golub, T.R., and Korsmeyer, S.J. (2002). MLL translocations specify a distinct gene expression profile that distinguishes a unique leukemia. Nat. Genet. *30*, 41–47. https://doi.org/10.1038/ng765.

34. Golub, T.R., Slonim, D.K., Tamayo, P., Huard, C., Gaasenbeek, M., Mesirov, J.P., Coller, H., Loh, M.L., Downing, J.R., Caligiuri, M.A., et al. (1999). Molecular Classification of Cancer: Class Discovery and Class Prediction by Gene Expression Monitoring. Science *286*, 531–537. https://doi.org/10.1126/science.286.5439.531.

35. Doll, S., Proneth, B., Tyurina, Y.Y., Panzilius, E., Kobayashi, S., Ingold, I., Irmler, M., Beckers, J., Aichler, M., Walch, A., et al. (2017). ACSL4 dictates ferroptosis sensitivity by shaping cellular lipid composition. Nat. Chem. Biol. *13*, 91–98. https://doi.org/10.1038/nchembio.2239.

36. Yuan, H., Li, X., Zhang, X., Kang, R., and Tang, D. (2016). Identification of ACSL4 as a biomarker and contributor of ferroptosis. Biochem. Biophys. Res. Commun. *478*, 1338–1343. https://doi.org/10.1016/j.bbrc.2016.08.124.

37. Kagan, V.E., Mao, G., Qu, F., Angeli, J.P.F., Doll, S., Croix, C.S., Dar, H.H., Liu, B., Tyurin, V.A., Ritov, V.B., et al. (2017). Oxidized arachidonic and adrenic PEs navigate cells to ferroptosis. Nat. Chem. Biol. *13*, 81–90. https://doi.org/10.1038/nchembio.2238.

38. Dixon, S.J., Lemberg, K.M., Lamprecht, M.R., Skouta, R., Zaitsev, E.M., Gleason, C.E., Patel, D.N., Bauer, A.J., Cantley, A.M., Yang, W.S., et al. (2012). Ferroptosis: An Iron-Dependent Form of Nonapoptotic Cell Death. Cell *149*, 1060–1072. https://doi.org/10.1016/j.cell.2012.03.042.

39. Ng, S.W.K., Mitchell, A., Kennedy, J.A., Chen, W.C., McLeod, J., Ibrahimova, N., Arruda, A., Popescu, A., Gupta, V., Schimmer, A.D., et al. (2016). A 17-gene stemness score for rapid determination of risk in acute leukaemia. Nature *540*, 433–437. https://doi.org/10.1038/nature20598.

40. Wang, J., Wang, H., Ding, Y., Jiao, X., Zhu, J., and Zhai, Z. (2024). NET-related gene signature for predicting AML prognosis. Sci. Rep. *14*, 9115. https://doi.org/10.1038/s41598-024-59464-y.

41. Ishizawa, J., Nakamaru, K., Seki, T., Tazaki, K., Kojima, K., Chachad, D., Zhao, R., Heese, L., Ma, W., Ma, M.C.J., et al. (2018). Predictive Gene Signatures Determine Tumor Sensitivity to MDM2 Inhibition. Cancer Res. *78*, 2721–2731. https://doi.org/10.1158/0008-5472.CAN-17-0949.

42. Cao, A., Li, H., Zhou, Y., Wu, M., and Liu, J. (2010). Long Chain Acyl-CoA Synthetase-3 Is a Molecular Target for Peroxisome Proliferator-activated Receptor δ in HepG2 Hepatoma Cells. J. Biol. Chem. *285*, 16664–16674. https://doi.org/10.1074/jbc.M110.112805.

43. Xu, H.E., Lambert, M.H., Montana, V.G., Parks, D.J., Blanchard, S.G., Brown, P.J., Sternbach, D.D., Lehmann, J.M., Wisely, G.B., Willson, T.M., et al. (1999). Molecular Recognition of Fatty Acids by Peroxisome Proliferator–Activated Receptors. Mol. Cell *3*, 397–403. https://doi.org/10.1016/S1097-2765(00)80467-0.

44. Li, Y.-J., Sun, L., Shi, Y., Wang, G., Wang, X., Dunn, S.E., Iorio, C., Screaton, R.A., and Spaner, D.E. (2017). PPAR-delta promotes survival of chronic lymphocytic leukemia cells in energetically unfavorable conditions. Leukemia *31*, 1905–1914. https://doi.org/10.1038/leu.2016.395.

45. Symeonidou, V., Jakobczyk, H., Bashanfer, S., Malouf, C., Fotopoulou, F., Kotecha, R.S., Anderson, R.A., Finch, A.J., and Ottersbach, K. (2021). Defining the fetal origin of MLL-AF4 infant leukemia highlights specific fatty acid requirements. Cell Rep. *37*, 109900. https://doi.org/10.1016/j.celrep.2021.109900.

46. Hermetet, F., Mshaik, R., Simonet, J., Callier, P., Delva, L., and Quéré, R. (2020). High-fat diet intensifies MLL-AF9-induced acute myeloid leukemia through activation of the FLT3 signaling in mouse primitive hematopoietic cells. Sci. Rep. *10*, 16187. https://doi.org/10.1038/s41598-020-73020-4.

47. Qi, D., Wang, J., Zhao, Y., Yang, Y., Wang, Y., Wang, H., Wang, L., Wang, Z., Xu, X., and Hu, Z. (2022). JMJD1C-regulated lipid synthesis contributes to the maintenance of MLL-rearranged acute myeloid leukemia. Leuk. Lymphoma *63*, 2149–2160. https://doi.org/10.1080/10428194.2022.2068004.

48. Kuo, H.-P., Wang, Z., Lee, D.-F., Iwasaki, M., Duque-Afonso, J., Wong, S.H.K., Lin, C.-H., Figueroa, M.E., Su, J., Lemischka, I.R., and Cleary, M.L. (2013). Epigenetic Roles of MLL Oncoproteins Are Dependent on NF-κB. Cancer Cell *24*, 423–437. https://doi.org/10.1016/j.ccr.2013.08.019.

49. Abdel-Aziz, A.K., Pallavicini, I., Ceccacci, E., Meroni, G., Saadeldin, M.K., Varasi, M., and Minucci, S. (2020). Tuning mTORC1 activity dictates the response of acute myeloid leukemia to LSD1 inhibition. Haematologica *105*, 2105–2117. https://doi.org/10.3324/haematol.2019.224501.

50. Zhou, X., Zhao, R., Lv, M., Xu, X., Liu, W., Li, X., Gao, Y., Zhao, Z., Zhang, Z., Li, Y., et al. (2023). ACSL4 promotes microglia-mediated neuroinflammation by regulating lipid metabolism and VGLL4 expression. Brain Behav. Immun. *109*, 331–343. https://doi.org/10.1016/j.bbi.2023.02.012.

51. Ma, Y., Nenkov, M., Berndt, A., Abubrig, M., Schmidt, M., Sandhaus, T., Huber, O., Clement, J.H., Lang, S.M., Chen, Y., and Gaßler, N. (2024). The Diagnostic Value of ACSL1, ACSL4, and ACSL5 and the Clinical Potential of an ACSL Inhibitor in Non-Small-Cell Lung Cancer. Cancers *16*, 1170. https://doi.org/10.3390/cancers16061170.

52. Stevens, B.M., Jones, C.L., Pollyea, D.A., Culp-Hill, R., D'Alessandro, A., Winters, A., Krug, A., Abbott, D., Goosman, M., Pei, S., et al. (2020). Fatty acid metabolism underlies venetoclax resistance in acute myeloid leukemia stem cells. Nat. Cancer *1*, 1176–1187. https://doi.org/10.1038/s43018-020-00126-z.

53. Thomas, D., Wu, M., Nakauchi, Y., Zheng, M., Thompson-Peach, C.A.L., Lim, K., Landberg, N., Köhnke, T., Robinson, N., Kaur, S., et al. (2023). Dysregulated Lipid Synthesis by Oncogenic IDH1 Mutation Is a Targetable Synthetic Lethal Vulnerability. Cancer Discov. *13*, 496–515. https://doi.org/10.1158/2159-8290.CD-21-0218.

54. Bahrami, E., Schmid, J.P., Jurinovic, V., Becker, M., Wirth, A.-K., Ludwig, R., Kreissig, S., Duque Angel, T.V., Amend, D., Hunt, K., et al. (2023). Combined proteomics and CRISPR–Cas9 screens in PDX identify ADAM10 as essential for leukemia in vivo. Mol. Cancer *22*, 107. https://doi.org/10.1186/s12943-023-01803-0.

55. Arafeh, R., Shibue, T., Dempster, J.M., Hahn, W.C., and Vazquez, F. (2025). The present and future of the Cancer Dependency Map. Nat. Rev. Cancer *25*, 59–73. https://doi.org/10.1038/s41568-024-00763-x.

56. The U.P.C.; Bateman, A., Martin, M.-J., Orchard, S., Magrane, M., Ahmad, S., Alpi, E., Bowler-Barnett, E.H., Britto, R., Bye-A-Jee, H., et al. (2023). UniProt: the Universal Protein Knowledgebase in 2023. Nucleic Acids Res. *51*, D523–D531. https://doi.org/10.1093/nar/gkac1052.

57. Fahy, E., Sud, M., Cotter, D., and Subramaniam, S. (2007). LIPID MAPS online tools for lipid research. Nucleic Acids Res. *35*, W606–W612. https://doi.org/10.1093/nar/gkm324.

58. Cancer Genome Atlas Research Network; Ley, T.J., Miller, C., Ding, L., Raphael, B.J., Mungall, A.J., Robertson, A.G., Hoadley, K., Triche, T.J., Jr., Laird, P.W., et al. (2013). Genomic and Epigenomic Landscapes of Adult De Novo Acute Myeloid Leukemia. N. Engl. J. Med. *368*, 2059–2074. https://doi.org/10.1056/NEJMoa1301689.

59. Tyner, J.W., Tognon, C.E., Bottomly, D., Wilmot, B., Kurtz, S.E., Savage, S.L., Long, N., Schultz, A.R., Traer, E., Abel, M., et al. (2018). Functional genomic landscape of acute myeloid leukaemia. Nature *562*, 526–531. https://doi.org/10.1038/s41586-018-0623-z.

60. Guo, Y., Dai, Y., Yu, H., Zhao, S., Samuels, D.C., and Shyr, Y. (2017). Improvements and impacts of GRCh38 human reference on high throughput sequencing data analysis. Genomics *109*, 83–90. https://doi.org/10.1016/j.ygeno.2017.01.005.

61. Subramanian, A., Tamayo, P., Mootha, V.K., Mukherjee, S., Ebert, B.L., Gillette, M.A., Paulovich, A., Pomeroy, S.L., Golub, T.R., Lander, E.S., and Mesirov, J.P. (2005). Gene set enrichment analysis: a knowledge-based approach for interpreting genome-wide expression profiles. Proc. Natl. Acad. Sci. USA *102*, 15545–15550. https://doi.org/10.1073/pnas.0506580102.

62. Dobin, A., Davis, C.A., Schlesinger, F., Drenkow, J., Zaleski, C., Jha, S., Batut, P., Chaisson, M., and Gingeras, T.R. (2013). STAR: ultrafast universal RNA-seq aligner. Bioinformatics *29*, 15–21. https://doi.org/10.1093/bioinformatics/bts635.

63. Liao, Y., Smyth, G.K., and Shi, W. (2019). The R package Rsubread is easier, faster, cheaper and better for alignment and quantification of RNA sequencing reads. Nucleic Acids Res. *47*, e47. https://doi.org/10.1093/nar/gkz114.

64. Love, M.I., Huber, W., and Anders, S. (2014). Moderated estimation of fold change and dispersion for RNA-seq data with DESeq2. Genome Biol. *15*, 550. https://doi.org/10.1186/s13059-014-0550-8.

65. Bolger, A.M., Lohse, M., and Usadel, B. (2014). Trimmomatic: a flexible trimmer for Illumina sequence data. Bioinformatics *30*, 2114–2120. https://doi.org/10.1093/bioinformatics/btu170.

66. Chong, J., Wishart, D.S., and Xia, J. (2019). Using MetaboAnalyst 4.0 for Comprehensive and Integrative Metabolomics Data Analysis. Curr. Protoc. Bioinforma. *68*, e86. https://doi.org/10.1002/cpbi.86.

67. Cerami, E., Gao, J., Dogrusoz, U., Gross, B.E., Sumer, S.O., Aksoy, B.A., Jacobsen, A., Byrne, C.J., Heuer, M.L., Larsson, E., et al. (2012). The cBio cancer genomics portal: an open platform for exploring multidimensional cancer genomics data. Cancer Discov. *2*, 401–404. https://doi.org/10.1158/2159-8290.CD-12-0095.

68. Conroy, M.J., Andrews, R.M., Andrews, S., Cockayne, L., Dennis, E.A., Fahy, E., Gaud, C., Griffiths, W.J., Jukes, G., Kolchin, M., et al. (2024). LIPID MAPS: update to databases and tools for the lipidomics community. Nucleic Acids Res. *52*, D1677–D1682. https://doi.org/10.1093/nar/gkad896.

69. Able, M., Kasper, M.-A., Vick, B., Schwach, J., Gao, X., Schmitt, S., Tizazu, B., Fischer, A., Künzl, S., Leilich, M., et al. (2025). Effective eradication of acute myeloid leukemia stem cells with FLT3-directed antibody-drug conjugates. Leukemia *39*, 632–642. https://doi.org/10.1038/s41375-024-02510-5.

70. Horlbeck, M.A., Gilbert, L.A., Villalta, J.E., Adamson, B., Pak, R.A., Chen, Y., Fields, A.P., Park, C.Y., Corn, J.E., Kampmann, M., and Weissman, J.S. (2016). Compact and highly active next-generation libraries for CRISPR-mediated gene repression and activation. eLife *5*, e19760. https://doi.org/10.7554/eLife.19760.

71. Rahimian, E., Koochak, M., Traikov, S., Schroeder, M., Brilloff, S., Schäfer, S., Kufrin, V., Küchler, S., Krüger, A., Mirtschink, P., et al. (2025). A quiescence-like/TGF-β1-specific CRISPRi screen reveals drug uptake transporters as secondary targets of kinase inhibitors in AML. Drug Resist. Updates *81*, 101242. https://doi.org/10.1016/j.drup.2025.101242.

72. Burocziova, M., Grusanovic, S., Vanickova, K., Kosanovic, S., and Alberich-Jorda, M. (2023). Chronic inflammation promotes cancer progression as a second hit. Exp. Hematol. *128*, 30–37. https://doi.org/10.1016/j.exphem.2023.09.002.

73. Kabadi, A.M., Ousterout, D.G., Hilton, I.B., and Gersbach, C.A. (2014). Multiplex CRISPR/Cas9-based genome engineering from a single lentiviral vector. Nucleic Acids Res. *42*, e147. https://doi.org/10.1093/nar/gku749.

74. Sanson, K.R., Hanna, R.E., Hegde, M., Donovan, K.F., Strand, C., Sullender, M.E., Vaimberg, E.W., Goodale, A., Root, D.E., Piccioni, F., and Doench, J.G. (2018). Optimized libraries for CRISPR-Cas9 genetic screens with multiple modalities. Nat. Commun. *9*, 5416. https://doi.org/10.1038/s41467-018-07901-8.

75. Doench, J.G., Fusi, N., Sullender, M., Hegde, M., Vaimberg, E.W., Donovan, K.F., Smith, I., Tothova, Z., Wilen, C., Orchard, R., et al. (2016). Optimized sgRNA design to maximize activity and minimize off-target effects of CRISPR-Cas9. Nat. Biotechnol. *34*, 184–191. https://doi.org/10.1038/nbt.3437.

76. Wurm, A.A., Brilloff, S., Kolovich, S., Schäfer, S., Rahimian, E., Kufrin, V., Bill, M., Carrero, Z.I., Drukewitz, S., Krüger, A., et al. (2023). Signaling-induced systematic repression of miRNAs uncovers cancer vulnerabilities and targeted therapy sensitivity. Cell Rep. Med. *4*, 101200. https://doi.org/10.1016/j.xcrm.2023.101200.

77. Müller, T., Kalxdorf, M., Longuespée, R., Kazdal, D.N., Stenzinger, A., and Krijgsveld, J. (2020). Automated sample preparation with SP 3 for low-input clinical proteomics. Mol. Syst. Biol. *16*, e9111. https://doi.org/10.15252/msb.20199111.

78. Burger, B., Vaudel, M., and Barsnes, H. (2021). Importance of Block Randomization When Designing Proteomics Experiments. J. Proteome Res. *20*, 122–128. https://doi.org/10.1021/acs.jproteome.0c00536.

79. Folch, J., Lees, M., and Sloane Stanley, G.H. (1957). A simple method for the isolation and purification of total lipides from animal tissues. J. Biol. Chem. *226*, 497–509.

80. Goracci, L., Tortorella, S., Tiberi, P., Pellegrino, R.M., Di Veroli, A., Valeri, A., and Cruciani, G. (2017). Lipostar, a Comprehensive Platform-Neutral Cheminformatics Tool for Lipidomics. Anal. Chem. *89*, 6257–6264. https://doi.org/10.1021/acs.analchem.7b01259.

81. Lange, M., Angelidou, G., Ni, Z., Criscuolo, A., Schiller, J., Blüher, M., and Fedorova, M. (2021). AdipoAtlas: A reference lipidome for human white adipose tissue. Cell Rep. Med. *2*, 100407. https://doi.org/10.1016/j.xcrm.2021.100407.

82. Pang, Z., Lu, Y., Zhou, G., Hui, F., Xu, L., Viau, C., Spigelman, A.F., MacDonald, P.E., Wishart, D.S., Li, S., and Xia, J. (2024). MetaboAnalyst 6.0: towards a unified platform for metabolomics data processing, analysis and interpretation. Nucleic Acids Res. *52*, W398–W406. https://doi.org/10.1093/nar/gkae253.

83. Mohamed, A., and Hill, M.M. (2021). LipidSuite: interactive web server for lipidomics differential and enrichment analysis. Nucleic Acids Res. *49*, W346–W351. https://doi.org/10.1093/nar/gkab327.

STAR★METHODS

KEY RESOURCES TABLE

REAGENT or RESOURCE	SOURCE	IDENTIFIER
Antibodies		
Anti-ACSL4 (A-5) Mouse mAb	Santa Cruz Biotechnology	Cat# sc-271800; RRID: AB_10715092
Anti-ACTB (4C2) Mouse mAb	Bio-Rad	Cat# VMA00048; RRID: AB_2923317
Rabbit Anti-Mouse-HRP	Abcam	Cat# ab6728; RRID: AB_955440
Bacterial and virus strains		
One Shot TOP 10 chemically competent cells	Thermo Fisher Scientific	Cat# C404010
Biological samples		
PDX-388	Bahrami et al.[54]	N/A
PDX-393	Bahrami et al.[54]	N/A
PDX-002	This Paper	N/A
Healthy human PBMCs	This Paper	N/A
MLL-AF9–transduced murine LKS cells	This Paper	N/A
Mouse bone marrow stromal cells (BMSCs)	This Paper	N/A
Chemicals, peptides, and recombinant proteins		
DMSO	Sigma-Aldrich	Cat# D2650
Hoechst 33342	Life Technologies	Cat# 40047
Lipofectamine 2000	Thermo Fisher Scientific	Cat# 11668019
PEIpro	Polyplus	Cat# 115-0015
Phosphatase inhibitor cocktail	Roche	Cat# 4906845001
Protease inhibitor cocktail	Sigma-Aldrich	Cat# P8340
Polybrene	Merck Millipore	Cat# TR-1003-G
Puromycin	Sigma-Aldrich	Cat# P8833
Radioimmunoprecipitation Assay (RIPA) buffer	Thermo Fisher Scientific	Cat# 89900
Sodium chloride (NaCl)	AppliChem	Cat# A2942,1000
Sodium deoxycholate	Sigma-Aldrich	Cat# D6750
Super optimal broth with catabolite repression (S.O.C.) medium	Invitrogen	Cat# 15544034
DMEM	Thermo Fisher Scientific	Cat# 12634028
DPBS	Thermo Fisher Scientific	Cat# 14190144
IMDM	Thermo Fisher Scientific	Cat# 12440053
RPMI 1640	Thermo Fisher Scientific	Cat# 11875093
StemPro™-34 SFM (1×)	Thermo Fisher Scientific	Cat# 10639011
Zombie Violet	BioLegend	Cat# 423113
Bio-Rad Protein Assay	Bio-Rad	Cat# 5000006
Pancoll	PAN Biotech	Cat# P04-60500
rm-GM-CSF	Immunotools	Cat# 12343125
rm-SCF	Immunotools	Cat# 12343325
rm-IL-3	Immunotools	Cat# 12340035
rh Flt3L	Immunotools	Cat# 11343305
rh-IL-6	Immunotools	Cat# 11340066
rh IL-3	Immunotools	Cat# 11340035
rh SCF	Immunotools	Cat# 11343325
rh TPO	Immunotools	Cat# 11344863

(*Continued on next page*)

Continued

REAGENT or RESOURCE	SOURCE	IDENTIFIER
Blp1	New England Biolabs	Cat# R0585S
BstX1	New England Biolabs	Cat# R0113S
T4 DNA Ligase (1 U/μL)	Invitrogen	Cat# EL0016
CutSmart Buffer	New England Biolabs	Cat# B7204
T4 DNA Ligase (1 U/μL) Buffer	Invitrogen	Cat# EL0016
20% Sodium dodecyl sulfate (SDS)	Sigma-Aldrich	Cat# 428018
30% Acrylamide mix	Bio-Rad	Cat# 1610156
4× Laemmli sample buffer	Bio-Rad	Cat# 1610747
Ampicillin	Sigma-Aldrich	Cat# A0166
Tris-HCl pH 8.0	Thermo Fisher Scientific	Cat# J22638.AE
Fetal bovine serum (FBS)	PAN-Biotech	Cat# P30-3306
Penicillin/streptomycin solution	Thermo Fisher Scientific	Cat# 15140122
Trypsin-EDTA (0.05%)	Thermo Fisher Scientific	Cat# 25300054
NP-40	Sigma-Aldrich	Cat# 492016
Sodium fluoride (NaF)	Sigma-Aldrich	Cat# S7920
Sodium orthovanadate (Na_3VO_4)	Sigma-Aldrich	Cat# S6508
Benzonase	Sigma-Aldrich	Cat# E1014
DNase I	Thermo Fisher Scientific	Cat# EN0521
Chloroform	Sigma-Aldrich/Merck	Cat# C2432
Methanol	Biosolve-Chemicals	Cat# 136841
Water (LC-MS grade)	Biosolve-Chemicals	Cat# 232178
Butylated Hydroxytoluene (BHT)	Sigma-Aldrich	Cat# B1378
SPLASH LIPIDOMIX internal standard	Avanti Polar Lipids Inc	Cat# 330707
Isopropanol	Biosolve-Chemicals	Cat# 162678
Acetonitrile	Biosolve-Chemicals	Cat# 012078
Ammonium formate	Sigma-Aldrich	Cat# 70221
Formic acid	Biosolve-Chemicals	Cat# 069141
Critical commercial assays		
SsoAdvanced# Universal SYBR® Green Super Mastermix	Bio-Rad	Cat# 1725272
BCA Protein Quantification Kit	Thermo Fisher Scientific	Cat# 23227
DNeasy Blood & Tissue Kit	Qiagen	Cat# 69506
Illumina stranded mRNA Prep, Ligation Kit	Illumina	Cat# 20020595
KAPA Taq EXtra HotStart ReadyMix	Roche	Cat# 07958935001
NextSeq 1000/2000 P2 Reagents (200 cycles) v3	Illumina	Cat# 20046812
Qubit™ dsDNA BR Assaykit	Thermo Fisher Scientific	Cat# Q32851
RevertAid First Strand cDNA Synthesis Kit	Life Technologies	Cat# K1622
RNase-Free DNase Set	Qiagen	Cat# 79256
RNeasy Mini Kit	Qiagen	Cat# 74104
Zymoclean Gel DNA Recovery Kit	Zymo Research	Cat# D4001
ZymoPURE II Plasmid Maxiprep Kit	Zymo Research	Cat# D4203
ZymoPURE Plasmid Miniprep Kit	Zymo Research	Cat# D4210
APC Annexin V Apoptosis Detection Kit with PI	BioLegend	Cat# 640932
MethoCult M3231	Stemcell Technologies	Cat# 03231
MethoCult H4230	Stemcell Technologies	Cat# 04230
dsDNA Broad range kit	Life Technologies	Cat# Q32850
NGS Fragment Kit (1-6000bp)	Agilent Technologies	Cat# DNF-477-0500

(*Continued on next page*)

Continued

REAGENT or RESOURCE	SOURCE	IDENTIFIER
Deposited data		
DepMap Public 23Q4 dataset	Arafeh et al.[55]	https://depmap.org/portal
UniProt human reference proteome (March 2023 release)	The UniProt Consortium et al.[56]	https://www.uniprot.org/
LIPID MAPS database	Fahy et al.[57]	https://www.lipidmaps.org/
TCGA-LAML RNA expression data	The Cancer Genome Atlas Research Network et al.[58]	https://portal.gdc.cancer.gov/
Beat AML RNA expression data	Tyner et al.[59]	https://www.vizome.org/aml
GRCh38.p14_genomic	Guo et al.[60]	https://www.ncbi.nlm.nih.gov/grc/human/data.
RNA sequencing data	Gene Expression Omnibus (GEO)	GEO: GSE274462
Mass spectrometry proteomics data	ProteomeXchange Consortium (PRIDE)	PRIDE: PXD072756
Processed transcriptomic data	This paper	Table S2
Processed proteomic data	This paper	Table S3
Processed lipidomic data	This paper	Table S4
Experimental models: Cell lines		
THP1	DSMZ	ACC 16; RRID: CVCL_0006
NOMO1	DSMZ	ACC 542; RRID: CVCL_1609
K562	DSMZ	ACC 10; RRID: CVCL_0004
MOLM16	DSMZ	ACC 777; RRID: CVCL_2120
MV4-11	DSMZ	ACC 102; RRID: CVCL_0064
U937	DSMZ	ACC 5; RRID: CVCL_0007
HEK293T	DSMZ	ACC 635; RRID: CVCL_0063
Experimental models: Organisms/strains		
Ly5.2 (CD45.2$^+$)	Jackson Laboratory	#000664
Ly5.1 (CD45.1$^+$)	Jackson Laboratory	#002014
Oligonucleotides		
sgRNAs	This Paper	STAR Methods: CRISPR interference
shRNAs	This Paper	STAR Methods: RNA interference
Primers	This Paper	STAR Methods: RNA isolation, cDNA synthesis and quantitative real-time PCR (qPCR)
Recombinant DNA		
psPAX2	Gift from Didier Trono	Addgene#12260
pMD2G.VSV.G	Gift from Didier Trono	Addgene#12259
pMSCV MLL-AF9-IRES-GFP	Gift from Daisuke Nakada	Addgene # 71443
pCL-Eco	Gift from Inder Verma	Addgene # 12371
pLV hUbC-dCas9 KRAB-T2A-GFP	Gift from Charles Gersbach	Addgene #67620
BFP-tagged pCRISPRia-v2	Gift from Jonathan Weissman	Addgene #84832
RFP-tagged pRSI12-U6-(sh)-UbiC-TagRFP-2A-Puro	Cellecta, Mountain View, CA, USA	NA
Software and algorithms		
GSEA_4.3.3	Subramanian et al.[61]	https://www.gsea-msigdb.org/gsea
CFX Maestro 2.3	Bio-Rad	NA
STAR 2.7.9a	Dobin et al.[62]	https://github.com/alexdobin/STAR
FACS Diva 8.0.2 and 8.0.1	BD Biosciences	NA
FlowJo v10.10.0	FlowJo	https://www.flowjo.com
GraphPad Prism V10.1.2	GraphPad Software	http://www.graphpad.com/
ImageJ	NIH	https://imagej.nih.gov/ij/

(*Continued on next page*)

Continued

REAGENT or RESOURCE	SOURCE	IDENTIFIER
Rsubread 2.18.0	Liao et al.[63]	https://bioconductor.org/packages/release/bioc/html/Rsubread.html
DESeq2 R package 1.20.0	Love et al.[64]	https://bioconductor.org/packages/release/bioc/html/DESeq2.html
FastQC	Babraham Bioinformatics	http://www.bioinformatics.babraham.ac.uk/projects/fastqc
Trimmomatic	Bolger et al.[65]	http://www.usadellab.org/cms/?page=trimmomatic
Spectronaut (v17.1.221229.55965)	Biognosys	https://www.biognosys.com/products/spectronaut
g:Profiler (functional enrichment)	Kolberg et al.[29]	https://biit.cs.ut.ee/gprofiler/
molbiotools Multiple List Comparator	MOLBIOTOOLS	https://molbiotools.com/listcompare.php
Lipostar2	Molecular Discovery	https://www.moldiscovery.com/lipostar-software/
MetaboAnalyst	Chong et al.[66]	https://www.metaboanalyst.ca/
LipidSuite	UNSW Sydney	https://lipidsuite.com
cBioPortal	Cerami et al.[67]	https://www.cbioportal.org/
R (v4.2.3)	R Foundation	https://www.r-project.org/
CRISPick	Broad Institute	https://portals.broadinstitute.org/gppx/crispick
LIPID MAPS database	Conroy et al.[68]	https://www.lipidmaps.org
Zotero 6.0.30	C+orporation for Digital Scholarship	https://www.zotero.org
Other		
VectorBuilder	VectorBuilder Inc.	https://vectorbuilder.com/
Polyvinylidene Fluoride (PVDF) membrane	Bio-Rad	Cat# 1620177
Qubit 2.0 Fluorometer	Life Technologies	Cat# Q32866
Fragment Analyzer 5200	Agilent Technologies	Cat# M5310AA
AssayMAP Bravo platform	Agilent Technologies	Cat# G5542BA
Orbitrap Exploris 480 mass spectrometer	Thermo Fisher Scientific	Cat# STEM-LE-1631-LC
Ultimate 3000 UPLC system	Thermo Fisher Scientific	Cat# 701455
Acclaim PepMap300 C18 cartridge	Thermo Fisher Scientific	Cat# 164535
Vanquish Horizon UHPLC system	Thermo Fisher Scientific	Cat# IQLAAAGABHFAPUMZZZ
Accucore C30 column, 150 mm × 2.1 mm, 2.6 μm	Thermo Fisher Scientific	Cat# 27826-152130
Orbitrap Exploris 240 mass spectrometer with HESI source	Thermo Fisher Scientific	Cat# IQLAAAGABHFAPUMZZZ

EXPERIMENTAL MODEL AND STUDY PARTICIPANT DETAILS

Animal studies

LKS cells were sorted from Ly5.2$^+$ WT C57BL/6 mice of both sexes (randomly selected) and transduced with MLL-AF9 retrovirus. 48 h after transduction, 1000 GFP+ MLL-AF9-infected cells were transplanted intravenously into Ly5.1$^+$ WT recipient mice. After 20 days (median survival), mice developed leukemia, and the BM was isolated and frozen for further use. Mice were maintained in the animal facility of the Institute of Molecular Genetics of the CAS. Mice were on a standard diet and a 12-h light–dark cycle with free access to food and water. The experiments were approved by the Ethical Committee of the Institute of Molecular Genetics of the CAS (Prague, Czech Republic) under approval number AVCR 4828/2025 PPZ.

Cell lines

Cell lines THP1, NOMO1, K562, MOLM16, MV4-11, U937, and HEK293T were obtained from DSMZ and continuously tested for mycoplasma and cross-contamination by Multiplex Cell Authentication (Multiplexion, Heidelberg, Germany). THP1, K562, and U937 were cultured in RPMI medium supplemented with 10% fetal bovine serum (FBS) and 1% penicillin/streptomycin, NOMO1 and MOLM16 were cultured in RPMI medium supplemented with 20% FBS and 1% penicillin/streptomycin, MV4-11 cells were cultured

in IMDM medium supplemented with 20% FBS and 1% penicillin/streptomycin, and HEK293T cells were cultured in DMEM supplemented with 10% FBS and 1% penicillin/streptomycin.

Patient-derived xenograft (PDX)

PDX388 and PDX393 were obtained from external sources,[54,69] while PDX-002 was established from a patient with AML for this study. PBMCs from healthy donors were isolated from apheresis material. All procedures involving human samples were conducted in accordance with institutional ethical guidelines and approved by the Ethics Committee of TU Dresden. For *in vitro* transduction, PDX cells were cultured in StemPro medium supplemented with 1% penicillin–streptomycin, 2mM L-glutamine, 100 ng/mL rh-SCF, 100 ng/mL rh-TPO, 50 ng/mL rh-FLT3L, 10 ng/mL rh-IL-6, and 10 ng/mL rh-IL-3. Following transduction, PDX cells were seeded for CFU assay in MethoCult H4230 (Stemcell Technologies, Vancouver, Canada) medium supplemented with 2mM L-glutamine, 100 ng/mL rh-SCF, 100 ng/mL rh-TPO, 50 ng/mL rh-FLT3L, 10 ng/mL rh-IL-6, and 10 ng/mL rh-IL-3.

METHOD DETAILS

Cancer dependency map (DepMap)

Analysis of CRISPR-Cas9-based dependency data was performed for ~1100 pan-cancer cell lines, including 24 AML cell lines. For these AML cell lines, corresponding mRNA expression generated by RNA sequencing, somatic mutational profiles, and gene fusion data were analyzed using datasets by the DepMap Portal (version 23Q4).[25] Raw data were downloaded and analyzed for each indicated cell line. Summarized data can be found in Table S1.

Gene Set Enrichment Analysis (GSEA) of DepMap data

Differentially expressed genes were calculated by comparing the median expression of log2-modified read counts between *ACSL4*-dependent (dependency score <-0.5, n = 10) and independent (dependency score >-0.5, n = 14) AML cell lines for all annotated genes. GSEA was performed using the GSEA_4.3.3 version according to the publisher's instructions.[61] The used cell line gene expression data can be found in Table S1.

sgRNA and shRNA cloning

ACSL4-targeting sgRNAs were cloned into the BFP-tagged pCRISPRia-v2 vector[70] (Addgene #84832), while *ACSL4*-targeting shRNAs were inserted into the RFP-tagged pRSI12-U6-(sh)-UbiC-TagRFP-2A-Puro vector (Cellecta, Mountain View, CA, USA). Complementary oligonucleotides containing the guide or hairpin sequences were synthesized, annealed, and ligated into the corresponding restriction-enzyme–digested vectors as previously described.[71] The ligation mixtures were transformed into E. coli Top10 cells, and positive colonies were selected on ampicillin-containing LB agar. Plasmid DNA was purified using a miniprep kit (Zymo Research, Irvine, CA, USA), and correct insert integration was verified by Sanger sequencing.

Production of lentiviral and retroviral particles

For Lentivirus production, packaging (psPAX2), envelope (pMD2G.VSV.G), and corresponding transfer plasmids were transfected into HEK293T cells using PEIpro transfection reagent (Polyplus, Illkirch, France) according to the manufacturer's protocol. Harvested lentiviral particles and 8 μg/mL polybrene were used for the transduction of AML cell lines, PDXs, and PBMCs. The vector pMSCV MLL-AF9-IRES-GFP was used to produce retroviral particles.[28] Retroviral supernatant and Lin-cKit+ Sca-1+ (LKS) transduction was performed as previously described.[72] Briefly, HEK293T cells were transfected with 10 μg of pMSCV MLL-AF9-IRES-GFP, 10 μg of pCL-Eco Retroviral Packaging Vector using Lipofectamine 2000 (Thermo Fisher Scientific, Waltham, MA, USA). After 4 h, the medium was replaced with fresh DMEM plus 10% FBS. After 24 and 48 h, retroviral supernatant was harvested and filtered through a 0.45-μm filter. Filtered virus supernatant was concentrated 50-fold by Centricon Plus-70 Centrifugal Filter (Sigma Aldrich, St. Louis, MO, USA), resuspended, and used for the transduction of sorted LKS cells.

CRISPR interference

dCas9-KRAB-expressing AML cells were generated by lentiviral transduction with pLV hUbC-dCas9 KRAB-T2A-GFP, a kind gift from Charles Gersbach (Addgene #67620).[73] Two sgRNAs targeting *ACSL4,* designed using CRISPick sgRNA designer from the Broad Institute,[74,75] and one non-targeting control sgRNA (NTC) were cloned into a BFP-tagged pCRISPRia-v2 vector, a gift from Jonathan Weissman (Addgene #84832).[70] sgRNAs were lentivirally transduced into dCas9-KRAB-expressing AML cells. Two days after transduction, the cells were separated into two fractions: one part was selected with 2 μg/mL puromycin for knockdown assessment, whereas the rest of the cells were cultured for the competition assay. Four sgRNAs were cloned into the backbone, and the knockdown was functionally tested. For further usage, the two sgRNAs with the highest knockdown capacity were selected. The following sgRNA sequences were used: *ACSL4* sgRNA1: ACCGCGTGCCCGCTAGCGCT; *ACSL4* sgRNA4: GCTTTCCGAGTG CCAGGCGC; NTC sgRNA: GCGATCTAATCGGAACTGTG.

RNA interference

Four shRNAs targeting either human *ACSL4* or murine *Acsl4* were designed using VectorBuilder (https://vectorbuilder.com/), and one scramble control shRNA, were cloned into the RFP-tagged pRSI12-U6-(sh)-UbiC-TagRFP-2A-Puro vector (Cellecta, Mountain View, CA, USA). Two days after transduction, the cells were separated into two fractions: one part was selected with 2 μg/mL puromycin for knockdown assessment, whereas the rest of the cells were cultured for the competition assay. Four shRNAs targeting each human *ACSL4* and murine *Acsl4* were cloned into the backbone, and the knockdown was functionally tested. For further usage, the two shRNAs with the highest knockdown capacity were selected. The following shRNA sequences were used: *ACSL4* shRNA1: GGCTCATGTGCTAGAACTGACAGCAGAGA; *ACSL4* shRNA4: GGCATTCCTCCAAGTAGACCAACGCCTTC; *Acsl4* shRNA1: GCCATGAAATTGGAGCGATTT; *Acsl4* shRNA3: CCTAGTTCAGAAGTTTCTATA; scramble shRNA: CAACAAGATGAAGAGCACCAA.

Flow cytometry-based competition assay

For flow cytometry analysis, cell lines were transduced with the respective sgRNAs or shRNAs. Four days post-transduction, cells were washed with PBS and measured with BD Fortessa cell analyzer (Becton Dickinson, Franklin Lakes, NJ, USA) to determine transduction efficiency, which also served as the day 0 baseline. Cells were reanalyzed every 7 days for growth assessment.

For the rescue experiment with polyunsaturated fatty acid (PUFA) supplementation, 4×10^5 cells were transduced with either a scramble control or two independent *ACSL4*-targeting shRNAs. Four days post-transduction, the percentage of RFP+ cells was measured (designated as day 0), and cells were subsequently treated with a defined PUFA cocktail containing docosahexaenoic acid (DHA, 22:6), eicosapentaenoic acid (EPA, 20:5), arachidonic acid (AA, 20:4), adrenic acid (AdA, 22:4), and docosapentaenoic acid (DPA, 22:5). PUFA concentrations were optimized based on prior XTT viability assays (THP1: DHA 25 μM, EPA 50 μM, AA 50 μM, AdA 50 μM, DPA 50 μM) (NOMO1: DHA 100 μM, EPA 100 μM, AA 100 μM, AA 100 μM, AdA 100 μM, DPA 50 μM). Cells were maintained in PUFA-supplemented medium throughout the experiment. Growth rescue was assessed via a competition assay, monitoring the relative percentage of RFP+ cells over time.

Apoptosis and cell cycle analysis

Apoptosis assay was performed using Annexin V-APC Kit (BioLegend, San Diego, CA, USA) according to the manufacturer's instructions. Zombie Violet (BioLegend, San Diego, CA, USA) was used for live/dead cell discrimination. Cell cycle analysis was performed by incubating 5×10^5 cells with 5 μg/mL Hoechst-33342 for 60 min at 37°C and subsequent flow cytometry analysis.

Colony-forming unit (CFU) assay

For the CFU assay in human cells, A total of 4×10^5 AML PDX cells or healthy PBMCs were transduced with two independent shRNAs targeting *ACSL4* or a scramble control in StemPro medium supplemented with 1% penicillin–streptomycin, 2mM L-glutamine, 100 ng/mL rh-SCF, 100 ng/mL rh-TPO, 50 ng/mL rh-FLT3L, 10 ng/mL rh-IL-6, 10 ng/mL rh-IL-3, and 8 μg/mL polybrene. After transduction, 1×10^4 cells were seeded per well in MethoCult H4230 (Stemcell Technologies, Vancouver, Canada) supplemented with 2mM L-glutamine, 100 ng/mL rh-SCF, 100 ng/mL rh-TPO, 50 ng/mL rh-FLT3L, 10 ng/mL rh-IL-6, and 10 ng/mL rh-IL-3. Images were acquired 14 days after seeding.

For the CFU assay in murine cells, healthy bone marrow mononuclear cells (BMMCs) were isolated from the bone marrow of C57BL/6 mice and separated using Pancoll (PAN Biotech, Aidenbach, Germany). 3×10^5 healthy BMMCs or MLL-AF9 cells were transduced with either scramble shRNA, *Acsl4* shRNA#1, or *Acsl4* shRNA#3 in IMDM supplemented with 20% FBS, 1% penicillin/streptomycin, 10 ng/mL rm-GM-CSF, 10 ng/mL rh-IL-6, 10 ng/mL rm-IL-3, and 50 ng/mL rm-SCF and 8 μg/mL polybrene. Cells were selected in 1 μg/mL puromycin 4 days after transduction for 3 days. After selection, 5×10^3 cells were seeded per well in MethoCult M3231 (Stemcell Technologies, Vancouver, BC, Canada) supplemented with 10 ng/mL rm-GM-CSF, 10 ng/mL rh-IL-6, 10 ng/mL rm-IL-3, and 50 ng/mL rm-SCF. Images were taken 10 days after seeding. All cytokines were purchased from Immunotools (Friesoythe, Germany).

MLL-AF9 cell transduction, transplantation, and peripheral blood analysis

On day 1, 3×10^5 MLL-AF9 Ly5.2+ BM cells were lentivirally transduced with *Acsl4* shRNA#1 or scramble shRNA (RFP+) using a MOI of 0.6. Cells were then incubated overnight at 37°C. On day 2, cells were washed and transplanted into non-irradiated Ly5.1 recipient mice. Each mouse received 5000 non-sorted cells. On day 3, the remaining cells were analyzed by flow cytometry, and the percentage of GFP+ and RFP+ infected cells was determined. Three weeks after transplantation, blood analysis was performed by flow cytometry, and the percentage of RFP+ cells gated from the GFP+ MLL-AF9 cells was determined. For the peripheral blood analysis, 2 experiments containing a total of 9 mice for each group were pooled. The transplanted mice were monitored closely for signs of leukemic progression. Upon leukemic development, mice were sacrificed, and the bone marrow and spleen were isolated and analyzed. Mouse survival was closely monitored (at least three times per week) during the entire experimental period.

Organ collection and flow cytometry analysis

Blood was isolated from the facial vein. Mice were sacrificed by cervical dislocation; the femur and tibia were isolated and crunched using a mortar and pestle to obtain cell suspensions. The spleen was isolated and was crunched using the piston of a syringe to obtain a cell suspension. The percentage of GFP+ and RFP+ cells was analyzed by flow cytometry.

Protein isolation and western blot

Western blots were performed as previously described.[76] Briefly, proteins were isolated by cell lysis in lysis buffer (150 mM NaCl, 50 mM Tris-HCl, 1% NP-40, 0.5% Sodium deoxycholate, and 0.1% SDS). Protein concentration was measured using Bio-Rad Protein Assay (Bio-Rad, Hercules, CA, USA). Denatured proteins were run on a Tris-Glycine SDS-Polyacrylamide gel according to the Bio-Rad protocol and transferred to PVDF membranes. Primary antibody incubation was performed at 4°C overnight. The secondary antibody was incubated for 1h at room temperature. The following primary antibodies were used: Anti-ACSL4 (A-5) Mouse mAb (sc-271800, Santa Cruz Biotechnology, Dallas, TX, USA), anti-ACTB (4C2) Mouse mAb (VMA00048, Bio-Rad, Hercules, CA, USA). Rabbit Anti-Mouse-HRP (ab6728, Abcam, Cambridge, UK) served as a secondary antibody.

RNA isolation, cDNA synthesis, and quantitative real-time PCR (qPCR)

RNA was isolated using the RNAeasy mini kit (Qiagen, Hilden, Germany). Reverse transcription (RT) was performed with the RevertAid First Strand cDNA Synthesis Kit (Life Technologies, Carlsbad, CA, USA) according to the manufacturer's instructions. For qPCR, SsoAdvanced# Universal SYBR® Green Super Mastermix (Bio-Rad, Hercules, CA, USA) was used. The following primers were included: *ACSL4*-for 5′- GCTATCTCCTCAGACACACCGA -3'; *ACSL4*-rev 5′- AGGTGCTCCAACTCTGCCAGTA -3'; *Acsl4*-for 5′- CCACACTTATGGCCGCTGTT -3'; *Acsl4*-rev 5′- GGGCGTCATAGCCTTTCTTG -3'; *ACTB*-for 5′-CATTGCTGACAGGATGCA GAAGG-3'; *ACTB*-rev 5′-TGCTGGAAGGTGGACAGTGAGG-3' (targeting human and murine *ACTB*/*Actb*).

Library preparation for RNA sequencing and data analysis

RNA libraries were prepared using the Illumina stranded mRNA Prep. Ligation Kit (Illumina, San Diego, CA, USA) according to the manufacturer's instructions. Briefly, mRNA was purified from 500 ng total RNA using oligo(dT) beads, poly(A)+ RNA was fragmented to 150 bp and converted into cDNA, and cDNA fragments were end-repaired, adenylated on the 3′ end, adapter-ligated, and amplified with 12 cycles of PCR. The quantity of the final libraries was validated using the dsDNA Broad range kit with the Qubit 2.0 Fluorometer (both Life Technologies, Carlsbad, CA, USA), and quality was validated using the NGS Fragment Kit (1-6000bp) on the Fragment Analyzer 5200 (both Agilent Technologies, Santa Clara, CA, USA). All barcoded libraries were pooled and sequenced 2 × 75bp paired-end on an Illumina NextSeq550 platform to obtain a minimum of 10 Mio reads per sample.

Quality control assessment of raw reads was performed using FastQC, followed by Trimmomatic trimming to remove low-quality sequences. The trimmed reads were then aligned to the reference genome using STAR version 2.7.9a. To facilitate the mapping process, a genome reference index was constructed using GRCh38.p14_genomic.gtf as the reference. Feature Counts were created by using Rsubread (2.18.0, https://bioconductor.org/packages/release/bioc/html/Rsubread.html), and differential expression analysis was performed using the DESeq2 R package (1.20.0, https://bioconductor.org/packages/release/bioc/html/DESeq2.html). DESeq2 output data was filtered for genes with a sum of read counts >60. GSEA was performed using the GSEA_4.3.3 version according to the publisher's instructions.[61] Summarized data can be found in Table S2.

Proteomics

Whole-cell proteins were isolated by cell lysis in lysis buffer (RIPA Lysis and Extraction Buffer (Thermo Fisher Scientific, Waltham, MA, USA) supplemented with 10 mM NaF, 1 mM Na3VO4, 250 U/mL benzonase, 10 U/mL DNase I, protease, and phosphatase inhibitors). Protein concentration was measured using Pierce BCA Protein Assay-Kit (Thermo Fisher Scientific, Waltham, MA, USA). An amount of 10 μg of protein was digested (trypsin) using an AssayMAP Bravo liquid handling system (Agilent Technologies, Santa Clara, CA, USA) running the autoSP3 protocol according to Müller et al.[77] The Liquid Chromatography with tandem mass spectrometry (LC-MS/MS) analysis was carried out on an Ultimate 3000 UPLC system (Thermo Fisher Scientific, Waltham, MA, USA) directly connected to an Orbitrap Exploris 480 mass spectrometer for a total of 120 min. Peptides were online desalted on a trapping cartridge (Acclaim PepMap300 C18, 5 μm, 300Å wide pore; Thermo Fisher Scientific, Waltham, MA, USA) for 3 min using 30 μL/min flow of 0.05% TFA in water. The analytical multistep gradient (300 nL/min) was performed using a nanoEase MZ Peptide analytical column (300Å, 1.7 μm, 75 μm × 200 mm, Waters, Milford, MA, USA) using solvent A (0.1% formic acid in water) and solvent B (0.1% formic acid in acetonitrile). For 102 min, the concentration of B was linearly ramped from 4% to 30%, followed by a quick ramp to 78%. After two minutes, the concentration of B was lowered to 2% and a 10-min equilibration step was appended. Eluting peptides were analyzed in the mass spectrometer using data-independent acquisition (DIA) mode. A full scan at 120k resolution (380–1400 m/z, 300% AGC target, 45 ms maxIT) was followed by 47 windows of variable isolation width (400–1000 m/z, 1000% AGC target, 30k resolution, 54 ms maxIT, centroid, 1 Da overlap) for fragment spectra acquisition. Collision energy was set at 28%. Each sample was followed by a wash run (40 min) to minimize carry-over between samples. Instrument performance throughout the course of the measurement was monitored by regular (approx. one per 48 h) injections of a standard sample and an in-house shiny application. All sample handling (sample preparation and LC-MS/MS analysis) has been performed in a block randomization order.[78] Analysis of DIA RAW files was performed with Spectronaut (Biognosys, version 17.1.221229.55965) in directDIA+ (deep) library-free mode. Default settings were applied with the following adaptations. Within the Pulsar Search in Peptides, the Max Peptide Length was set to 35, in Result Filters, the Peptide Charge was enabled, and the Max Charge set to 6, and the Min Charge set to 2. Within DIA Analysis under Identification, the Precursor PEP Cutoff was set to 0.01, the Protein Qvalue Cutoff (Run) set to 0.01, and the Protein PEP Cutoff set to 0.05. In Quantification, the Proteotypicity Filter was set to Only Protein Group Specific, the Cross-Run Normalization was disabled, the Quantification window was set to Not Synchronized, and the Major Group Quantity was set to Sum peptide quantity. The data was

searched against the human proteome from Uniprot (human reference database with one protein sequence per gene, containing 20,591 unique entries from the first of March 2023) and the contaminants FASTA from MaxQuant (246 unique entries from twenty-second of December 2022). For subsequent analysis, proteins detected in only one out of the eight samples were excluded from analysis. Protein PG intensities were transformed (x+1) to perform a log fold change analysis and calculate the *p*-value with an unpaired, two-tailed Student's *t* test. Summarized data can be found in Table S3. Up- and downregulated transcripts and proteins were compared using the multiple list comparator by molbiotools (https://molbiotools.com/listcompare.php), and functional enrichment analysis of overlapping genes was performed using g:Profiler.[29]

Lipidomics

For the lipidomic analysis, 2×10^6 cells from five replicates were extracted using chloroform-methanol-water-based liquid-liquid extraction.[79] All extraction solvents contained 1 μg/mL butylated hydroxytoluene (BHT) and were pre-cooled on ice before use. Briefly, SPLASH LIPIDOMIX (Avanti Polar Lipids Inc, 3 μL) internal lipid standards were added to each sample, incubated on ice for 15 min, followed by the addition of methanol (300 μL) and chloroform (600 μL). Samples were vortexed, incubated at 4°C for 1h on a rotary shaker, and phase separation was induced by the addition of water (100 μL), followed by vortexing, incubation at 4°C (10 min), and centrifugation (1000 × g, 10 min, 4°C). The organic phase was collected and dried in a vacuum concentrator.

For LC-MS/MS analysis, lipids were resuspended in 50 μL of isopropanol, centrifuged, and 40 μL were transferred to glass vials. Lipids (1.5 and 3 μL for positive and negative ion mode analysis, respectively) were separated by reverse phase chromatography (Accucore C30 column; 150 mm × 2.1 mm 2.6 μM 150 Å, Thermo Fisher Scientific) using a Vanquish Horizon UHPLC system (Thermo Fisher Scientific) coupled on-line to an Orbitrap Exploris 240 mass spectrometer (Thermo Fisher Scientific) equipped with a HESI source. Lipids were separated at a flow rate of 0.3 mL/min (column temperature 50°C) by a the following gradient: 0–5 min, 10 to 12,5% B; 5–20 min, 12,5 to 80%; 20–24 min, 80 to 95%; 24–27 min, 95 to 100%; 27–32 min, isocratic 100%; 32–40 min, re-equilibration at 10% B. Eluent A was acetonitrile: water (50:50, v/v, both ULC/MS-CC/SFC grade, Biosolve-Chemicals) and Eluent B was 2-propanol:acetonitrile: water (85:10:5, v/v/v), both containing 5 mM ammonium formate (MS grade, Sigma-Aldrich) and 0.1% formic acid (ULC/MS-CC/SFC grade, Biosolve-Chemicals). Full MS settings were the following: spray voltage – 3500 V, sheath gas – 40 arb units, aux gas – 10 arb units, sweep gas – 1 arb unit, ion transfer tube – 300°C, vaporizer temperature – 370°C, EASY-IC run-start, default charge state – 1, resolution at m/z 200–120.000, scan range – m/z 200–1200, normalized AGC target – 100%, maximum injection time – auto, RF lens – 35%. Data-dependent acquisition (DDA) was based on a cycle time (1.3 s) at a resolution of 30.000, isolation window – 1.2 m/z, normalized stepped collision energies – 17,27,37%, AGC target – 100%, maximum injection time – 54 ms.

Lipid identification was performed using Lipostar2.[80] Features with isotopic pattern and MS/MS spectrum were matched against the LIPID MAPS database and selected based on automatic approval (3–4 stars). After manual approval based on the established LC-MS/MS lipid identification strategy,[81] lipid identities and chromatographic peak areas were exported and used for further analysis. Peak areas were normalized according to lipid standard abundances of the SPLASH LIPIDOMIX and cell count. Heatmap and scores plot were generated using MetaboAnalyst.[82] Differential analysis comparing *ACSL4* knockdown to the control was performed using the univariate analysis by Lipid Suite.[83] Data on total unsaturated bonds of different lipid classes were also extracted from the LipidSuite analysis. Summarized data can be found in Table S4.

Analysis of external datasets

We analyzed mRNA expression from 173 patients with AML (TCGA-LAML) from the Cancer Genome Atlas (TCGA) database[58] and 649 patients diagnosed with AML from the Beat AML study.[31] Raw data were downloaded using the cBioportal online tool (https://www.cbioportal.org/) and further processed according to the median expression of the studied genes. GSEA was performed using the GSEA_4.3.3 version according to the publisher's instructions.[61] Summarized data can be found in Table S5.

QUANTIFICATION AND STATISTICAL ANALYSIS

We used the Wilcoxon rank sum test (also known as the Mann-Whitney U test) or the two-sided unpaired *t* test, respectively, to determine the statistical significance of experimental results. The results were represented as the mean ± SD from at least three independent experiments unless otherwise stated. Statistical significance was assessed using the Log rank (Mantel–Cox) test for mouse experiments and the Gehan–Breslow–Wilcoxon test for survival data from patients with AML, depending on the distribution of survival events over time. Statistical tests were performed with GraphPad Prism version 10.1.2 or R version 4.2.3.